JGR Biogeosciences

RESEARCH ARTICLE
10.1029/2025JG008978

Transition Zones at the Changing Coastal Terrestrial-Aquatic Interface

Kaizad F. Patel[1], Avni Malhotra[1], Cooper G. Norris[1,2], Sophia A. McKever[1], Devon M. Fields[3], Jared I. Musci[4], Sreejata Bandopadhyay[1], Ben Bond-Lamberty[1], Xingyuan Chen[1], Donnie J. Day[5], Kennedy O. Doro[5], Etienne Fluet-Chouinard[1], Marci Garcia[1], Kenneth M. Kemner[6], Fausto Machado-Silva[5], Nate McDowell[1], Kendalynn A. Morris[1], Allison Myers-Pigg[1,5], Edward J. O'Loughlin[6], Teri O'Meara[7], Roberta B. Peixoto[5], Stephanie C. Pennington[1], Peter Regier[1], Roy Rich[7], Kenton A. Rod[1,5], Benjamin Sulman[7], Peter Thornton[7], Nicholas Ward[1], Stephanie J. Wilson[8], Michael N. Weintraub[1,5], J. Patrick Megonigal[8], and Vanessa L. Bailey[1,5]

[1]Pacific Northwest National Laboratory, Richland, WA, USA, [2]CME Associates, Inc., East Syracuse, NY, USA, [3]California State Polytechnic University, Humboldt, Arcata, CA, USA, [4]Ohio State University, Columbus, OH, USA, [5]University of Toledo, Toledo, OH, USA, [6]Argonne National Laboratory, Lemont, IL, USA, [7]Oak Ridge National Laboratory, Oak Ridge, TN, USA, [8]Smithsonian Environmental Research Institute, Edgewater, MD, USA

Key Points:

- We investigated variability in soil biogeochemistry across coastal systems to determine key parameters that may be transferable across different coastal regions
- Analytes such as C, Fe, Al, and P are important sources of regional variability in soil chemistry
- Transition zones do not always represent the intermediate point along the upland-to-marsh gradient and often show unique biogeochemical properties

Correspondence to:
K. F. Patel,
kaizad.patel@pnnl.gov

Citation:
Patel, K. F., Malhotra, A., Norris, C. G., McKever, S. A., Fields, D. M., Musci, J. I., et al. (2025). Transition zones at the changing coastal terrestrial-aquatic interface. *Journal of Geophysical Research: Biogeosciences*, *130*, e2025JG008978. https://doi.org/10.1029/2025JG008978

Received 28 MAR 2025
Accepted 25 SEP 2025

Author Contributions:
Conceptualization: Kaizad F. Patel, Kenneth M. Kemner, Allison Myers-Pigg, Teri O'Meara, Nicholas Ward, Michael N. Weintraub, Vanessa L. Bailey
Data curation: Kaizad F. Patel, Ben Bond-Lamberty, Etienne Fluet-Chouinard, Stephanie C. Pennington, Peter Regier
Formal analysis: Kaizad F. Patel, Avni Malhotra, Vanessa L. Bailey
Funding acquisition: Ben Bond-Lamberty, Xingyuan Chen, Kenneth M. Kemner, Nicholas Ward, Michael

Abstract Coastal soils are a significant but highly uncertain component of global biogeochemical cycles. These systems experience spatial and temporal variability in biogeochemical processes, driven by marsh-to-upland gradients and hydrological fluctuations. These fluctuations make it difficult to understand and predict biogeochemical processes in these highly dynamic systems. We studied coastal soil biogeochemistry and its variability (a) at regional scales and (b) across transects from upland forest to marsh, in two contrasting regions—Lake Erie, a freshwater lacustrine system, and Chesapeake Bay, a saltwater estuarine system. Salinity-related analytes were a key source of variability in soil biogeochemistry, not just in the saltwater system, but surprisingly, also in the freshwater system. We had hypothesized linear trends in biogeochemical parameters along the TAI—however, contrary to expectations, transition soils were not consistently intermediate between upland and marsh endmembers; the non-monotonic trends of C, P, Fe along our transects suggest that these do not behave as expected and may be difficult to model and predict—thus these are key analytes to study in our regions. Rapidly changing soil factors across coastal gradients (e.g., Ca, K, CEC, and TS) may act as precursors to ecosystem shifts. Our comprehensive soil characterization represents a snapshot of a single timepoint of surface soils and provides essential data for mechanistic modeling of ecosystem dynamics across coastal transects.

Plain Language Summary Coastal soils are important for global cycles of nutrients and chemicals, but their behavior is not well understood. These soils vary greatly both over space and time, influenced by changes from marsh to upland areas and by water movement and disturbances. We studied soil variability in two different regions: Lake Erie, a freshwater system, and Chesapeake Bay, a saltwater system. We found that salt-related factors significantly affected soil variability in both areas, which was unexpected for the freshwater system. Surprisingly, transition zones between upland and marsh did not always have intermediate soil properties. Elements such as carbon (C), phosphorus (P), and iron (Fe) showed complex patterns in these transition zones. Understanding the rapid changes in these soil factors can help predict shifts in ecosystems. Our detailed study of coastal soils provides essential information for modeling and understanding how these ecosystems function and change.

1. Introduction

Coastal terrestrial aquatic interfaces (TAIs) include a wide range of upland and marsh ecosystems that are exposed to inundation of varying salinity on diel to seasonal, or even decadal timescales. Coastal TAI soils are responsible for globally significant carbon pools and fluxes but remain a key unknown in our understanding of the global carbon cycle (Friedlingstein et al., 2022; Regnier et al., 2022; Rosentreter et al., 2021; Saunois et al., 2020, 2024). Future sea level rise and large lake level variability are expected to shift both the spatial (e.g., shifting coastal forests into marshes, McDowell et al., 2022; Molino et al., 2023) and temporal attributes (e.g., extreme hydrological events such as storm surges, Yan et al., 2020) of these ecosystems. Coastal TAI soils exhibit strong

N. Weintraub, J. Patrick Megonigal, Vanessa L. Bailey
Investigation: Kaizad F. Patel, Cooper G. Norris, Sophia A. McKever, Devon M. Fields, Jared I. Musci, Donnie J. Day, Marci Garcia, Edward J. O'Loughlin, Kenton A. Rod, Stephanie J. Wilson
Methodology: Kaizad F. Patel
Resources: Donnie J. Day, Kendalynn A. Morris, Stephanie J. Wilson, J. Patrick Megonigal
Software: Kaizad F. Patel
Supervision: Michael N. Weintraub, Vanessa L. Bailey
Validation: Kaizad F. Patel
Visualization: Kaizad F. Patel
Writing – original draft: Kaizad F. Patel, Avni Malhotra
Writing – review & editing: Avni Malhotra, Sreejata Bandopadhyay, Ben Bond-Lamberty, Xingyuan Chen, Donnie J. Day, Kennedy O. Doro, Etienne Fluet-Chouinard, Kenneth M. Kemner, Fausto Machado-Silva, Nate McDowell, Kendalynn A. Morris, Allison Myers-Pigg, Edward J. O'Loughlin, Teri O'Meara, Roberta B. Peixoto, Peter Regier, Roy Rich, Kenton A. Rod, Benjamin Sulman, Peter Thornton, Nicholas Ward, Stephanie J. Wilson, Michael N. Weintraub, J. Patrick Megonigal, Vanessa L. Bailey

spatial gradients arising from the hydrogeomorphic features of their associated estuaries or lakes (Hoitink & Jay, 2016). Increases in soil saturation, and changes in redox potential and nutrient levels can affect the establishment of plants (Crain et al., 2004) and microbial communities (Córdova-Kreylos et al., 2006; Ramírez-Flandes et al., 2019), ultimately influencing biogeochemical cycles (Guimond et al., 2025; Machado-Silva et al., 2024; Noe et al., 2013; Patel et al., 2024; Wilson & Megonigal, 2025). However, understanding how these gradients and hydrological fluctuations influence regional biogeochemistry remains a crucial question to be addressed.

The consequences of these hydrological disturbances across TAI soils and their outcomes for carbon and nutrient transformations remain poorly understood (O'Meara et al., 2024; Ward et al., 2020), in part because research efforts have historically focused on either marsh or upland systems in isolation and less so on the dynamic transitional zone between the two (Byrd et al., 2016; Morris et al., 2022; A. J. Smith & Goetz, 2021; Vahsen et al., 2024). Moreover, aside from coastal flooding, terrestrial hydrological inputs from adjacent upland systems can exert a strong control on redox patterns in coastal marshes (Machado-Silva et al., 2024; Montalvo et al., 2024). Temporally dynamic redox conditions and steep spatial gradients make coastal soils biogeochemically distinct from inland soils (Regier et al., 2021; Ward et al., 2020), yet the degree and extent of this difference, and possible range of soil biogeochemical variability across coastal TAI gradients, remain unclear.

Coastal transitional systems such as ghost forests represent a functional intermediate between upland and marsh endmembers and are a crucial but challenging location to constrain biogeochemical function (Seyfried et al., 2023). These forests experience strong hydrodynamic fluctuations and gradually rising water levels that can cause tree die-off and inward migration of marsh vegetation over longer timescales (Ding et al., 2023; Kirwan & Gedan, 2019; Langston et al., 2017; McDowell et al., 2022; W. Wang et al., 2022). These changes can have drastic effects on soil biogeochemical processes, including loss of nutrients (Herbert et al., 2015; Noe et al., 2013) and shifting greenhouse gas balances (Petrakis et al., 2017; F. Wang et al., 2019). The unique mix of degraded forests (dead/dying trees), fluctuating hydrology, and invading marsh vegetation can result in distinct biogeochemical characteristics in transitional forests. Indeed, some studies have found increased soil carbon and nitrogen concentrations in these "ghost forests" (H. Chen et al., 2023), and increased emissions of greenhouse gases (F. Wang et al., 2019), although these patterns are inconsistent across studies (Craft, 2012; Noe et al., 2013).

Knowledge of coastal transitional forest biogeochemistry is an important component of understanding and scaling the functional consequences of rapidly changing ecosystems. At the scale of individual field sites, assumptions about unmeasured biogeochemical parameters and rates (Shiklomanov et al., 2020) often underpin models of interconnected hydrology across upland to marsh gradients (Li et al., 2024; Ward et al., 2020). Important unanswered questions include: what amount of bias is introduced into model projections of ecosystem carbon cycling by using spatially invariant values for soil parameters governing biogeochemical process rates and plant physiology (Sinha et al., 2023) across the upland-to-marsh gradient? Do freshwater versus saltwater systems have different dominant drivers? And do key processes in transitional systems differ from those of gradient end members? Answering these questions and improving confidence in models' projections of coastal transitional forests, requires spatially detailed observational data across a wide range of coastal ecosystems, both saline and freshwater, and gradients in between.

Here, we quantified soil biogeochemical patterns and sources of variability across the coastal TAI in two contrasting coastal regions—Western Lake Erie (a freshwater lacustrine system, hereafter referred to as "Erie") and Chesapeake Bay (a saltwater estuarine system, referred to as "Chesapeake")—to examine how coastal TAI soils varied (a) at regional scales and (b) across forest-to-marsh gradients. We generally use the term "coastal" to refer to both the estuarine and lacustrine systems because they share similar upland to marsh hydrologic gradients and represent the shoreline of continental-scale water bodies. To capture TAI spatial gradients comprehensively, we sampled surface soils across transects spanning coastal marshes and forests and their intermediate transition areas (Figure 1). We quantified 20 soil analytes describing carbon and other macronutrients, micronutrients, mineralogy, and marine or agricultural-related elements (Appendix A2) to determine how similar or different soils were from the two regions. Our goal was to understand patterns and soil biogeochemistry at TAIs in two strongly contrasting coastal systems; identify key sources of variability; and determine if there were unique sources for Erie versus Chesapeake regions. We hypothesized that: (H1) sources of the variability in soil biogeochemical parameters would differ for saltwater (Chesapeake Bay) versus freshwater (Lake Erie) coastal soils, with pedogenic and agriculture-related variables (e.g. Al, Ca, N, P) more important in Erie, and salinity-related

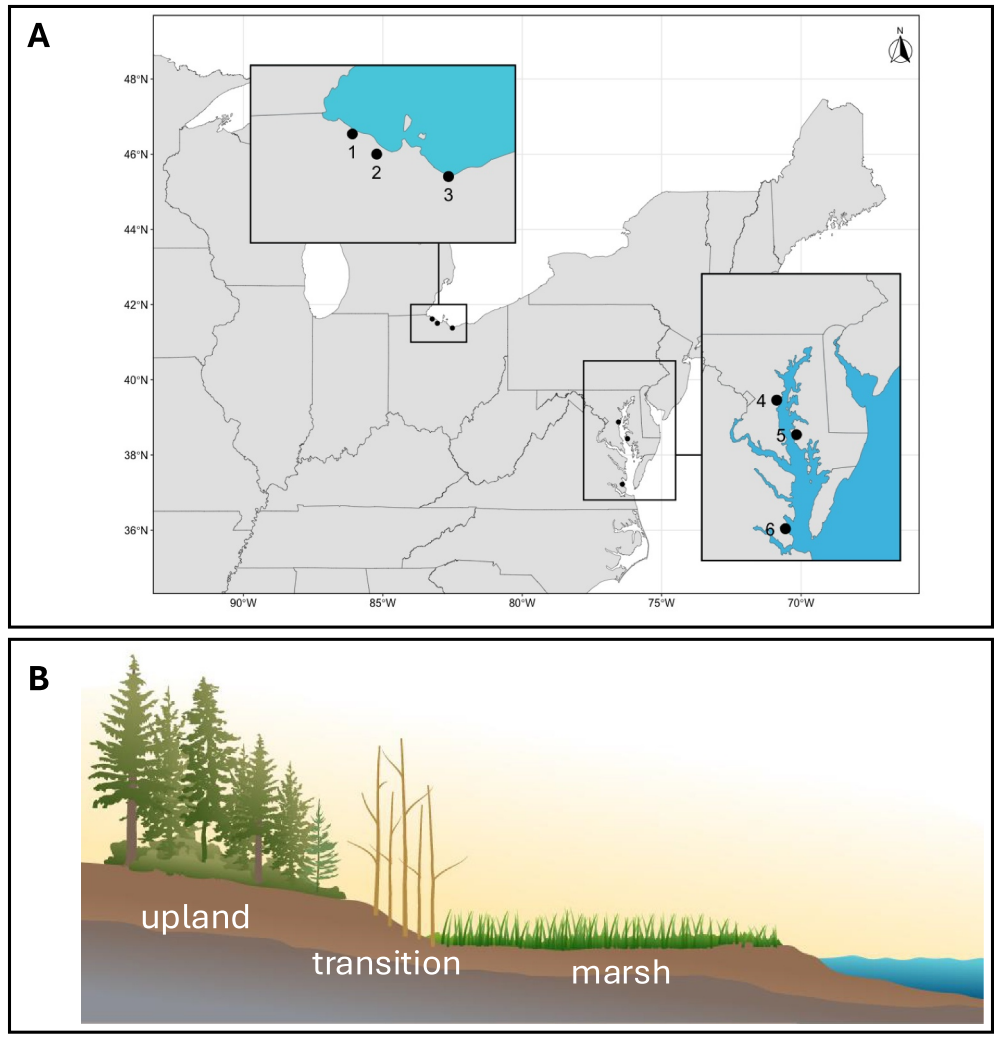

Figure 1. (a) Site locations described in this paper. Lake Erie sites: (1) CRC—Crane Creek and (2) PTR—Portage River are in the Western Basin, and (3) OWC—Old Woman Creek is in the Central Basin of Lake Erie. Chesapeake Bay sites: (4) GCW—Global Change Research Wetland, (5) MSM—Moneystump Marsh, and (6) GWI—Goodwin Islands. (b) Transverse coastal transect, with upland, transition, and marsh zones. At each zone, soils were collected from the surface (O or A horizon, $n = 8$).

variables (e.g., Na, Cl, SO_4) more important in Chesapeake; and (H2) transition soil characteristics would be quantitatively intermediate between marsh and upland end members for each region. The experimental design represents a snapshot of a single timepoint, but it provides a useful framework to track ecosystem function and key variables in our study regions.

2. Materials and Methods

2.1. Site Description

This research was conducted at six sites in the Chesapeake Bay and the Western Lake Erie Basin (Ward et al., 2025) (Figure 1a). These two regions were selected because of their extensive coastlines and contrasting TAI systems—Lake Erie represents a freshwater, lacustrine coastal system, whereas Chesapeake Bay represents an estuarine coastal system. As such, these regions help us understand biogeochemical processes occurring in contrasting environments, including different salinities, hydroperiods, land use histories, and nutrient loads. All of our sites are characterized by shallow elevation gradients from healthy upland forest, through a transitional zone with a mix of live and dying and dead trees (ghost forests), to a coastal marsh, with coastal surface waters

connected to the lake or estuary. These gradients, including the presence of ghost forests, are ubiquitous in low-lying TAIs in both the Great Lakes and the Mid-Atlantic. Specific sites, transects, and zones were chosen based on criteria that included hypothesis testing and logistical considerations. In Chesapeake Bay, the primary criterion for sites was the salinity of the adjacent estuary, while in Lake Erie, it was soil mineralogy (see below). Chief among secondary criteria was site access and security to support extensive monitoring equipment for related aspects of the present study. All sites were deemed sufficiently representative of their respective regions based on local expert knowledge.

2.1.1. Lake Erie

Western Lake Erie is the most dynamic part of the lake because it is the shallowest region and receives the largest inflows of water, sediments, and nutrients from the Detroit, Maumee, Sandusky, and other rivers (Moorhead et al., 2008). The TAI across this region has coastal marshes surrounded by tile-drained agricultural lands. Coastal marshes are located within conservation areas dominated by native and invasive herbaceous species (Herdendorf et al., 2006), shrubs, and broadleaf trees.

In the Western Lake Erie region, we selected three sites that span an east-west gradient in soil mineralogy, allowing us to examine how soil water retention affects biogeochemical and ecological processes. Old Woman Creek (OWC), the furthest-east site, is in the western edge of Lake Erie's Central Basin and has better drained soils containing more sand than the more clayey soils of Portage River (PTR) and Crane Creek (CRC) in the Western Basin. The Erie soils were all Entisols, Inceptisols, or Alfisols with surface A horizons and no O horizons. The soil order and horizon type efficiently capture and summarize features such as texture, organic matter (OM) content, chemical characteristics, and site history that strongly influence the ecology and biogeochemical properties of our systems. This information is also the basic contextual data necessary to build a transferable understanding of coastal soils. All three sites are considered to be within the Huron-Erie Lake Plains Ecoregion and consist of poorly drained glacial and lacustrine deposits overlying Silurian and Devonian carbonate bedrock (Ehosioke et al., 2024; Ohio, 2012). Glacial advance and retreat during the late Wisconsinan glacial period have caused this region to be primarily flat and uniform. Elevation gradients are relatively shallow (Table 1), potentially inhibiting groundwater discharge into adjacent coastal marshes, although this may vary between sites in fine-textured soils that retain water (PTR and CRC) and better-drained sandy soils (OWC). Terrestrial habitats in the OWC Reserve are former agricultural fields in various stages of succession and hardwood forests (Herdendorf et al., 2006).

2.1.2. Chesapeake Bay

The Chesapeake Bay is one of the largest estuaries in the world, with 18,804 km of convoluted fractal shoreline arising from its origin as a drowned river valley. The western shore of the Chesapeake Bay has relatively steep topographic gradients, fine-textured soils, and broad-leaf forests in contrast to the eastern shore which is relatively flat with sandy soils and evergreen forests (Lowrance et al., 1997; Maryland-DNR, 2015). Similar contrasts in topography, soils, and dominant tree species exist on the western shore with subestuaries near the head of the Bay or headwaters of major tributaries having relatively steeper topography, finer soils, and broadleaved vegetation. The Chesapeake Bay has over 100 subestuaries, which have relatively shallow bathymetry and have high ratios of TAI shoreline to estuarine water volume, resulting in strong TAI coupling. These systems are hotspots of biological and biogeochemical activity; are sensitive to extreme rainfall events that transport nearly the entire annual load of nutrient-laden sediments from land into the Chesapeake Bay (Jordan et al., 1997; Palinkas et al., 2014); and are also where the impacts of storm surges and sea level rise are most severe (Noe et al., 2020).

In the Chesapeake Bay, we selected three sites along the Bay's surface water salinity gradient that range from oligo- to meso-haline (Global Change Research Wetland, GCW and Moneystump Marsh, MSM), and polyhaline (Goodwin Islands, GWI). The two mesohaline sites differ in their geomorphic setting with GCW located on the western shore and MSM on the eastern shore. The two western shore sites also differ with GCW toward the head of the Bay and GWI toward the mouth of the Bay. The GCW soils were Inceptisols and Ultisols under deciduous vegetation with surface A horizons and relatively poorly developed O horizons. By contrast, the other two Chesapeake sites were Ultisols under pine vegetation, with well-developed surface O horizons. The Chesapeake marshes in this study are tidal marshes dominated by C3 sedges and C4 grasses, with root-dominated Oe horizons for the top 20 inches.

Journal of Geophysical Research: Biogeosciences
10.1029/2025JG008978

Table 1
Site Characteristics for the Western Lake Erie Sites

	Crane Creek (CRC)			Portage River (PTR)			Old Woman Creek (OWC)		
	Upland	Transition	Marsh	Upland	Transition	Marsh	Upland	Transition	Marsh
Latitude (N)	41.61524	41.62192	41.62185	41.50148	41.502723	41.50174	41.37618	41.376017	41.376445
Longitude (E)	−83.22889	−83.23815	−83.2389	−83.04611	−83.045662	−83.04372	−82.50685	−82.507507	−82.509024
Elevation (m)	175.2	175.1	175.1	175.7	175.4	174.9	179.7	175.2	174.8
MAT (°C)[a]		10.64			10.64			10.64	
MAP (cm)		113.2			113.2			113.2	
Vegetation	Mixed broadleaf forest dominated by *Quercus alba* (white oak)	Mixed broadleaf forest dominated by *Quercus bicolor* (swamp white oak)	Freshwater emergent marsh dominated by fragmented zones of *Typha latifolia*, *Peltandra virginica* (green arrow arum), *Phragmites australis* (common reed), and *Phalaris arundinacea* (reed canary grass)	Mixed broadleaf forest dominated by *Carya ovata* (shagbark hickory)	Mixed broadleaf forest dominated by *Carya ovata*	Freshwater emergent marsh dominated by fragmented zones of *Typha latifolia* (bulrush), *Phragmites australis*, and *Phalaris arundinacea*	Mixed broadleaf forest dominated by *Quercus rubra* (northern red oak)	Mixed broadleaf forest dominated by *Quercus rubra*	Freshwater emergent marsh dominated by fragmented zones of *Saurus cernuus* (lizard's tail) and *Phalaris arundinacea*
Parent material[b]	Fine Textured Lacustrine Deposits	Fine Textured Lacustrine Deposits	Fine Textured Lacustrine Deposits	Fine Textured Lacustrine Deposits	Fine Textured Lacustrine Deposits	Fine Textured Lacustrine Deposits	Fine Textured Lacustrine Deposits	Fine Textured Lacustrine Deposits	Fine Textured Lacustrine Deposits
Soil Series	Toledo silty clay and Nappannee silty clay loam (Mollic Endoaquepts and Aeric Epiaqualfs)	Toledo silty clay, flooded (Mollic Endoaquepts)		Toledo silty clay (Mollic Endoaquepts)	Toledo silty clay, flooded (Mollic Endoaquepts)		Zurich, Bixler (Oxyaquic and Aquic Arenic Hapludalfs)	Holly silt loam (Fluvaquentic Endoaquepts)	Fluvaquents, frequently flooded
Horizon sampled	A	A	A	A	A	A	A	A	A

[a]Data from https://climatereanalyzer.org/. [b]Data from https://soilexplorer.net/.

2.2. Transect Design and Soil Sampling

Each site was characterized by a distinct elevation gradient (Figure 1b) across which we established a transect for soil and vegetation sampling. The transect consisted of three distinct zones: upland forest with relatively deep water tables, dry soils, healthy trees, and oxic soils; transitional forest with occasional inundation due to storm surges and extreme high tides, and characterized by higher water tables, periods of hypoxic or anoxic soils, and stressed or dead trees (ghost forests); and marsh, which is characterized by long periods of soil saturation or flooding, dominantly anoxic soils, and herbaceous plant species adapted to such conditions. The upland-to-marsh transects spanned 100–200 m in length across the six sites, except for CRC, at 1,000 m (Tables 1 and 2, Appendix A1).

Soils were sampled from all Erie sites in December 2021 and from Chesapeake sites MSM-GWI in May 2022 and from Chesapeake site GCW in September 2022. Samples were collected across the three transect locations for each site. At each transect location, soil samples were collected from 8 to 9 spatially distributed discrete locations over an area of 200–1,000 m^2 to account for spatial variability. Samples were collected from the surface (O or A horizon, top 5–10 cm). The samples were shipped to the laboratory on blue ice and kept refrigerated at 4°C until ready for processing and analysis.

2.3. Laboratory Processing, Extractions, and Analyses

In the laboratory, the soil samples were sieved and homogenized (4 mm mesh for A and B horizons, 6 mm mesh for O horizons). The marsh samples from CB had extremely high root content and were therefore not sieved. All samples were then processed and extracted for the various analyses described below. These analyses are also summarized in Appendix A2.

Gravimetric water content was determined by drying field-moist samples for 24 hr (105°C for A and B horizons and 60°C for O horizons). Gravimetric water content was calculated as the percentage weight loss following drying, normalized to oven-dry weight. *Organic matter content* was determined using the loss on ignition method. Oven-dry samples were combusted in a muffle furnace at 450°C for 12 hr. Organic matter content was calculated as the percentage weight loss following combustion, normalized to oven-dry weight. *Total C, N, S* were determined on freeze-dried samples by catalytic combustion using elemental analyzers VarioMax Cube (total C, N) and Rapid CS Cube (total S (TS)) (Elementar Analysensysteme GmbH). *pH and specific conductance* were determined by shaking freeze-dried soil with deionized MilliQ water (1:10 w:v) for 30 min and then measuring with a Milwaukee MW802 PRO probe. *Exchangeable base cations (Ca, Mg, Na, K) and acid cations (Al)* were extracted using 1 M NH_4Cl (1:5 w:v ratio). Samples were shaken with the extracting solution at 200 rpm for 1 hr, followed by centrifuging at 7,000 rcf and 20°C for 15 min, and then vacuum-filtering using Büchner funnels with Whatman 42 filter paper. The elemental concentrations were measured using ICP-OES (PerkinElmer Optima 8300) and normalized to the dry weight of soil used. Effective cation exchange capacity (meq/100 g soil) was calculated as the sum of charges for Ca, Mg, Na, K, and Al.

Extractable inorganic N (NH_4-N and NO_3-N) was obtained by shaking soil samples with 2 M KCl (1:5 w:v ratio) at 200 rpm for 1 hr, followed by centrifuging at 7,000 rcf and 20°C for 15 min, and then vacuum-filtering using Büchner funnels with Whatman 42 filter paper. NH_4-N was measured using a Lachat FIA QuikChem and NO_3-N was measured colorimetrically using Griess reagent at the Oregon State University Soil Analytical Laboratory. *Water extractable organic C* (WEOC) was obtained by shaking soil with deionized MilliQ water (1:5 w:v ratio) at 200 rpm for 1 hr, followed by centrifuging at 7,000 rcf and 20°C for 15 min, and then filtering using 0.45 µm PES syringe filters. WEOC was measured as non-purgeable organic carbon using a Shimadzu TOC-L analyzer. These water extracts were also used for WEIC (water extractable inorganic carbon) measurements (Shimadzu TOC-L) and water-extractable anion measurements for chloride and sulfate (Dionex ICS-3000 chromatograph).

Extractable phosphorus was obtained by shaking soil samples with Mehlich-III reagent (1:5 w/v ratio) at 200 rpm for 1 hr, followed by centrifugation at 7,000 rcf and 20°C for 15 min. The supernatant was pipetted out and analyzed for ortho-phosphate colorimetrically using the Murphy-Riley ascorbic acid method (ammonium molybdate + antimony potassium tartrate + ascorbic acid), with absorbance measured at 880 nm on a plate reader (Mehlich, 1984). *Extractable iron* was obtained by shaking soil samples with 0.5 M HCl (1:10 w/v ratio) at 200 rpm for 1 hr, followed by centrifuging at 7,000 rcf and 20°C for 15 min. The supernatant was pipetted out and analyzed for iron colorimetrically using the ferrozine method (ferrozine reagent + 10% ascorbic acid), with absorbance measured at 562 nm on a plate reader (Huang & Hall, 2017; Viollier et al., 2000).

Journal of Geophysical Research: Biogeosciences 10.1029/2025JG008978

Table 2
Site Characteristics for the Chesapeake Bay Sites

	Global Change Research Wetland (GCW)			Moneystump Marsh (MSM)			Goodwin Islands (GWI)		
	Upland	Transition	Marsh	Upland	Transition	Marsh	Upland	Transition	Marsh
Latitude (N)	38.874445	38.874440	38.874948	38.43085	38.43042	38.42923	37.21927	37.21928	37.21892
Longitude (E)	−76.551667	−76.551110	−76.549995	−76.22622	−76.22708	−76.22739	−76.40851	−76.40937	−76.41002
Elevation (m)	7.09	1.21	0.24	0.68	0.48	0.29	1.03	0.79	0.68
Salinity of surface water (psu)		5–10			5–10			18–25	
MAT (°C)[a]		14.03			14.03			17.53	
MAP (cm)		126.8			126.8			141.8	
Vegetation	Mixed deciduous tree community including *Acer rubrum* (red maple), *Fagus grandifolia* (American beech) and *Quercus alba/falcata* (white oak/southern red oak)	Mixed deciduous tree community including *Acer rubrum, Fagus grandifolia* and *Quercus alba/falcata*	Tidal marsh dominated by *Spartina patens* (saltmeadow cordgrass), *Distichlis spicata* (desert saltgrass)	*Pinus taeda* (loblolly pine) conifer forest	*Pinus taeda* conifer forest	Salt marsh dominated by *Spartina patens Distichlis spicata and Schoenoplectus robustus*	*Pinus taeda* forest	*Pinus taeda* forest with a substantial *Phragmites australis* understory	Salt marsh dominated by *Spartina patens*, *Distichlis spicata*
Parent material[b]	Glauconite-bearing loamy fluviomarine deposits	Loamy alluvium	Herbaceous plant material over marine coastal deposits	Loamy Fluvio-Deltaic Coastal Sediments	Clayey Fluvio-Deltaic Coastal Sediments	Clayey Fluvio-Deltaic Coastal Sediments	Marine deposits	Marine deposits	Marine deposits
Soil Series	Collington and Annapolis, fine sandy loam (Typic Hapludults)	Widewater and Issue, silt loam (Fluvaquentic Endoaquept and Dystrudeptss)	Mispillon and Transquaking, mucky peat	Elkton mucky silt loam (Typic Endoaquults)	Sunken mucky silt loam, occasionally flooded, tidal (Typic Endoaqualfs)	Honga peat, very frequently flooded, tidal (Terric Sulfihemists)	Dragston fine sandy loam (Aeric Endoaquults)	Nimmo fine sandy loam (Typic Endoaquults)	Axis fine sandy loam (Typic Sulfaquents)
Horizon sampled	A	A	A	O	O	O	O	O	O

[a]Data from https://climatereanalyzer.org/. [a]Data from https://soilexplorer.net/.

Mineralogy was determined using X-ray diffraction (XRD) analysis at the Environmental Molecular Sciences Laboratory. Samples were freeze-dried and then ground in a ball mill. The quantitative XRD patterns (QXRD) of bulk samples were collected from powders packed into zero-background well holders using a Rigaku SmartLab SE diffractometer, employing a Bragg-Brentano geometry with a Cu X-ray source (λ = 1.5418 Å), a variable divergence slit, and a high-speed D/teX Ultra 250 1D detector. The samples were scanned between 2 and 100°2θ at intervals of 0.01°2θ, scanning at 2°2θ/min. The proportion of minerals was quantified by the Rietveld method using TOPAS (v6, Bruker AXS). This method combines calculated XRD patterns from the substituent minerals to provide the best fit with the observed pattern. For each mineral the scale factor, cell parameters (constrained within ca. 0.5% of the expected values), and crystallite size (constrained between 50 and 500 nm) were refined. For platy minerals (e.g., mica minerals), a preferred orientation correction was also refined. The scale factors from the Rietveld refinement were used to determine the relative quantities of the minerals, which are presented scaled to a total of 100%. Unidentified or amorphous compounds were ignored.

Bulk density was calculated using intact soil rings (5 cm height × 5 cm diameter), as the ratio of oven-dry mass of soil to its volume in the ring. *Water retention curves* were generated using the HYPROP device (METER Group). Intact soil cores (HYPROP rings, 5 cm height × 5 cm diameter) were saturated with water and placed on HYPROP devices fitted with tensiometers. The tension and soil weight were continuously recorded as the samples were air-dried at room temperature. Water retention curves were fitted using the Van Genuchten equation (van Genuchten, 1980), and additional readings for the dry end of the curve were determined using the WP4C Soil Water Potential Sensor. *Particle size analysis* was performed using the hydrometer method. 40 g of soil was subjected to chemical (50 mg/L sodium hexametaphosphate, HMP) and physical dispersion, after which the volume was made up to 1,000 mL. Hydrometer measurements were taken at 90 min and 24 hr to calculate the clay fraction. The sample was then sieved through a 53 μm sieve to determine the sand fraction. The soil texture was determined based on the percentage of sand-silt-clay. Prior to the particle size analysis, OM was removed using 30% hydrogen peroxide. Because of the high organic content in O horizon soils (from Chesapeake Bay), we did not perform particle size analysis on these. This analysis was performed only on the mineral soils (A horizon).

2.4. Data and Statistical Analysis

2.4.1. Exploratory Analysis

We used multivariate Principal Components Analysis (PCA), PERMANOVA, and hierarchical clustering analysis to determine overall groupings in the chemistry data across the regions, sites, and transects (Figures 2 and 3). We used the PC1 loadings data to determine significant factors that explained variability for each region (Figure 4). We performed correlation analysis as part of the data exploration and excluded highly correlated variables from the PCA, PERMANOVA, and cluster analysis (Appendix A3). The variables we excluded were SO_4, NO_3-N, CEC, K, total N, Mg, and OM, leaving us with 13 variables in our analysis.

2.4.2. Analyzing Individual Analytes

To determine general trends in analyte concentrations along the transect, we scaled each analyte for each site to a 0–1 range (Figure 5). We did this to easily detect and compare various analytes across a range of units and magnitudes. Where analytes followed a trend of upland < transition < marsh (e.g., TS at all sites), the upland received a value of 0 and marsh 1, with transition intermediate. For the reverse trend (upland > transition > marsh), the upland received a value of 1 and marsh 0, with transition intermediate. In some cases, however, the analytes did not follow a monotonic trend, and the transition values were in fact greater than upland and marsh; in those instances, the transition received a value of 1, identifying it as a hotspot (e.g., Fe, WEOC, P, Figure 5).

We used linear mixed-effects models (LME) and ANOVA to determine trends in each analyte across the transect and sites (Appendix A7). For LMEs, we used site as the random variable. Statistical significance was determined at $\alpha = 0.05$.

2.4.3. Software and Packages Used

All data analysis was performed using R v4.21, with packages *dplyr* v1.1.4 for data cleaning and processing, *ggplot2* v3.5.1, PNWColors v0.1.0, and *soilpalettes* v0.1.0 for data visualization. We used the package *ggcorrplot* v0.1.4 for correlation analysis; *factoextra* v1.0.7, stats, *vegan* v2.6-4, and *ggbiplot* v0.55 for multivariate analyses;

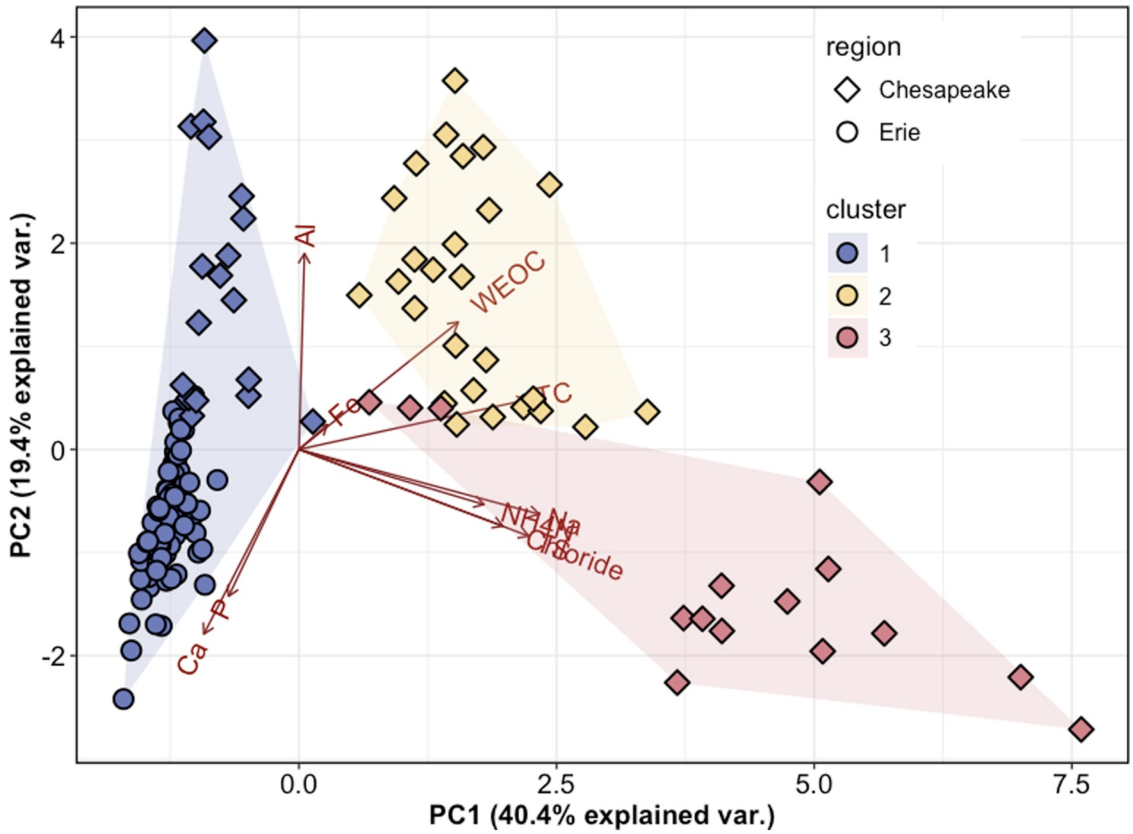

Figure 2. Principal components analysis for all surface soil samples. The three shaded regions represent the three hierarchical clusters. Cluster 1 contains all soils from Lake Erie, and upland and transition soils from GCW in Chesapeake Bay; Cluster 2 contains MSM and GWI upland and transition soils; Cluster 3 contains all Chesapeake marshes.

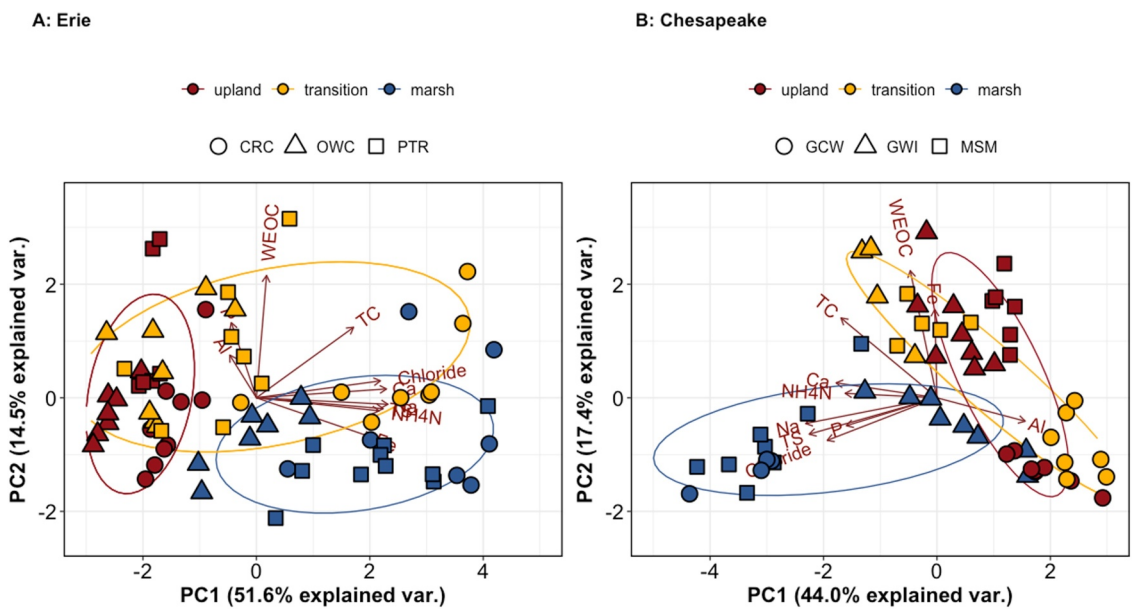

Figure 3. Principal component analysis for all surface soil samples, split by region. (a) Sites from the Lake Erie and (b) Chesapeake Bay regions. The ellipses represent 95% confidence intervals for the three transect positions (upland forest, transitional forest, and marsh).

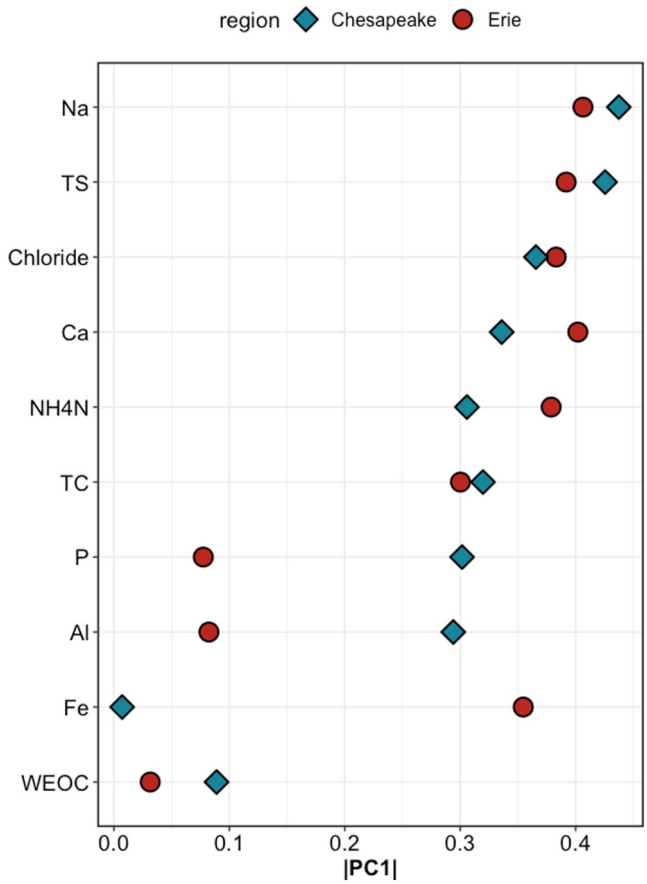

Figure 4. PC1 loadings from Figure 3. The *x*-axis represents the PC1 loadings from the Principal Components Analysis (PCA) of soil chemistry, where a higher value on the *x*-axis signifies a larger weight in the PCA and represents a greater contribution of that analyte to the overall variability within the PCA biplots in Figure 3. Analytes such as Na, TS, and Cl were strong contributors of variability in the PCA for both Chesapeake and Erie; Al and P were stronger contributors in Chesapeake, whereas Ca, NH_4-N, and Fe were stronger contributors in Erie.

and *agricolae* v1.3-5 for univariate analyses. All data and R scripts are available on GitHub (https://github.com/COMPASS-DOE/cmps-soil_characterization) and archived on ESS-DIVE (Patel et al., 2025).

3. Results

3.1. Regions Vary in Soil Biogeochemical Patterns

Overall, region (Chesapeake Bay vs. Lake Erie) accounted for 29% of total variation in soil biogeochemical analytes ($F = 173$), whereas soil horizon (O vs. A) accounted for 16% ($F = 96.7$) and transect position (upland vs. transition vs. marsh) accounted for 9% of the variation ($F = 28.6$) (PERMANOVA, $p < 0.001$ for all). In a 2D ordination space using PCA (Figure 2), PC1 accounted for ~40% of the total variability, associated mostly with salinity-related analytes (Na, TS, specific conductance, Cl) and carbon (TC). The secondary axis of variability, PC2, explained 19% of the variability and was driven primarily by Ca, pH, Al (analytes associated with acidity/alkalinity), and P (agricultural inputs). From hierarchical cluster analysis, the Erie soils formed a single cluster, whereas the Chesapeake soils showed greater dispersion across both axes, suggesting overall greater variability among the Chesapeake soils (Figure 2). Interestingly, upland and transition soils at GCW (a Chesapeake site) clustered with the Erie soils. The other two Chesapeake sites were split across clusters, with upland and transition soils grouped together and marshes grouped together (Figure 2).

Given the strong differences between the two regions, we analyzed transect-scale patterns in each region separately to determine how the transition zones compared with their respective upland and marsh end-members. The two regions exhibited clear separation by transect position (Figure 3), but also different sources of variability in soil biogeochemical parameters (Figure 4). For Erie, the upland and marsh soils formed two distinct groups in the PCA ordination space, with the transitional soils occupying the space between them (Figure 3a). In contrast, for Chesapeake, there was notable overlap between the upland and transitional soils, which were grouped together. Meanwhile, the marshes formed a separate distinct group (Figure 3b). The sole exception were a few samples from the GWI marsh that grouped with the upland and transition soils.

We quantified the relative contribution of each analyte to the overall variability in soils, inferred using PC1 loadings (Figure 4). Analytes with a higher loading contributed more to overall variability—Na, TS, and Cl (salinity related) strongly contributed to overall variability for both regions. Ca and Fe were stronger contributors of variability in the PCA of Erie soils; whereas Al and P were the main contributors in the Chesapeake soils.

3.2. Transitions Are Not Always the Intermediate Value

We investigated biogeochemical patterns at the site level to determine how the transitional soils compared with the upland and marsh endmembers, and to see if these patterns were consistent across analytes and regions. Within-transect patterns were not consistent across all the analytes (Figures 5 and 6). Analytes such as TS and Na followed a linear trend along the transect, with upland < transition < marsh, for both regions (i.e., upland received a normalized value of 0 and marsh had a normalized value of 1). Cl followed a similar pattern for four of the six sites; notably, at GWI, which is the most saline of our Chesapeake sites, marsh soils had the lowest Cl concentrations along the transect (Figure 5, Appendix A6). In some cases, the analytes did not follow a linear trend, and the transition values were greater than upland and marsh. Examples of this pattern included WEOC in the Erie soils, Fe in the Chesapeake soils, and P in OWC, an Erie site (Figures 5 and 6). NH_4-N trends were inconsistent across the Chesapeake sites—upland < transition < marsh in MSM, but upland < marsh < transition in GWI and transition < upland < marsh in GCW.

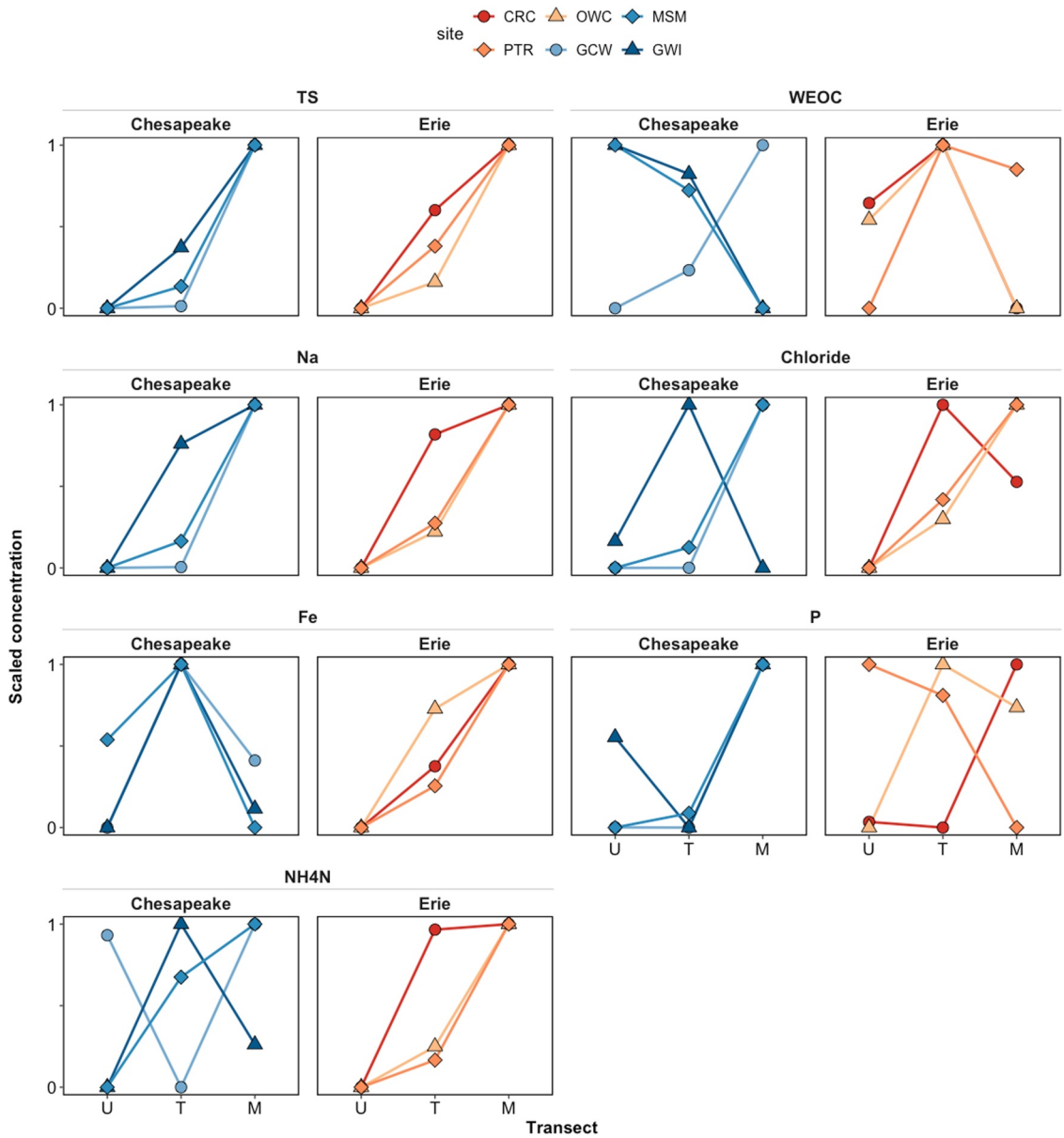

Figure 5. Scaled values of select analytes across transect positions. Each line represents a single site. Values shown here represent scaled median concentrations to show relative trends along the transect. All values were scaled to 0–1, and the relative values reflect trends within each transect. For some analytes (e.g., TS) the upland soils had a value of 0 and the marsh 1, indicating progressive trends along the transect (upland < transition < marsh). Whereas others (P, Fe, WEOC) showed non-monotonic trends, with transition concentrations significantly greater than in the upland and marsh. Raw (un-scaled) values are available in Appendix A7.

4. Discussion

4.1. Soil Characteristics Modified by Salinity and Vegetation Drive Biogeochemical Patterns

Our PERMANOVA and PCA results highlight the strong importance of region in understanding coastal biogeochemical patterns. While salinity is an obvious difference between the Chesapeake and Erie regions, there could be other factors at play, such as soil and vegetation type, as we discuss below.

Our initial analyses (Figure 2) suggest a strong influence of salinity on overall biogeochemistry patterns, although soil type may also play an important role. Despite their proximity to the saline Chesapeake Bay, GCW upland and transition soils were more similar to the freshwater Erie soils than to other Chesapeake soils (cluster 1 in Figure 2). Among the Chesapeake sites, GCW experiences low salinity (~6 psu), and therefore this result may not be

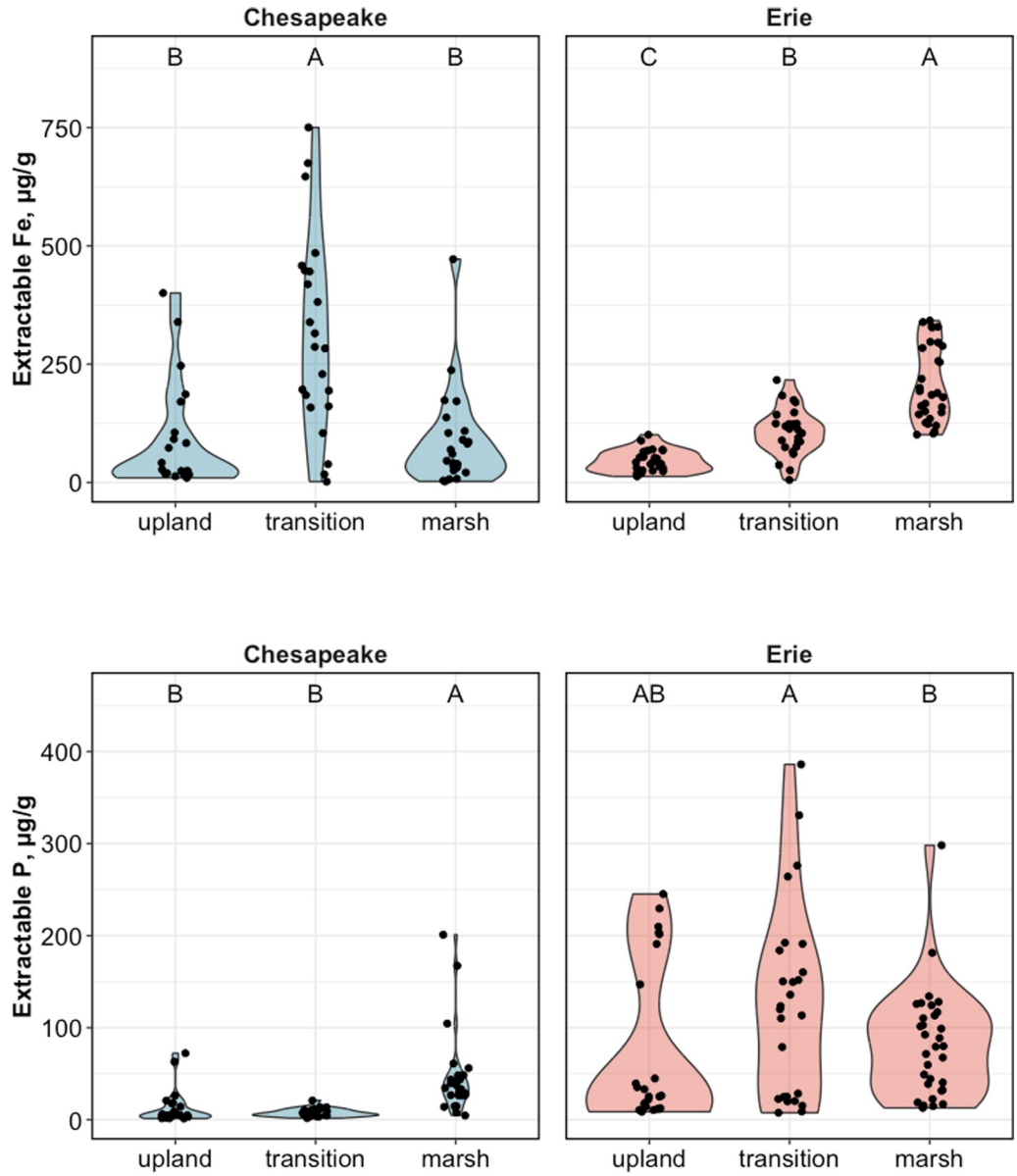

Figure 6. Concentrations of extractable Fe and P across transect zones. Multiple sites are grouped per transect positions. Extractable Fe in the Erie soils showed a linear increase along the transect, with upland < transition < marsh. In the Chesapeake soils, however, Fe concentrations in the transitional soils were significantly greater than in upland and marsh. Extractable P in the Erie also showed non-monotonic trends, with concentrations in the transition greater than in the upland and marsh. Positions labeled with different letters are statistically different (Tukey HSD, $\alpha = 0.05$).

surprising despite its physical location. GCW is also distinct among Chesapeake sites because the upland and transition sites occur on a steep elevation gradient (Appendix A4) resulting in little influence of estuarine water beyond the marsh. GCW soils are fine-textured and the site is dominated by deciduous vegetation; characteristics shared by all upland and transition zones in Erie. By contrast, the forested sites at MSM and GWI are relatively coarse-textured and dominated by evergreen conifer vegetation. These results illustrate that the interplay of geomorphic, hydrologic, and ecological factors is necessary to consider for spatial scaling and modeling of coastal soils.

Dominant tree type may have also influenced soil horizon development at our sites, with relatively well-developed surface O horizons under evergreen species compared with mineral A horizons under deciduous species (Weil & Brady, 2016). Further, soil horizon characteristics can influence additional physical properties

such as bulk density and water retention; these analyses were not part of our PCAs, but we observed strong differences between O and A horizon soils for these properties (Appendix A5). The fact that soil horizon influenced soil chemistry is not surprising, but our analysis highlights horizons as an important source of variability and necessary to consider in coastal soil modeling (De Feudis et al., 2022; Patel et al., 2021).

Patterns of soil biogeochemistry across the marsh-upland gradient also differed strongly between the two regions. Transitional forests in Erie showed properties intermediate between the upland and marsh endmembers, whereas for the Chesapeake soils, transition soils were more similar to the upland (Figure 3). This pattern in the Chesapeake soils was unexpected; we expected greater distinctions between upland and transition soils in this region because the exposure of transitional forests to saltwater is known to impact soil chemistry (Hopple et al., 2022; Morrissey et al., 2014; Weissman & Tully, 2020). One explanation lies in the assumption, based on our space-for-time-substitution design, that transition zone soils were upland soils relatively recently and retain certain soil characteristics that change slowly. This suggests that the legacy of soil forming factors is a fundamental constraint on the rate at which certain soil characteristics respond to hydrologic and biogeochemical change (Oliver et al., 2021; Tank et al., 2020; Walker et al., 2010).

4.2. Regions Differ in Sources of Soil Biogeochemical Variability

The PC1 loadings in Figure 4 allow us to identify analytes with the most variability in our soils. Interestingly, the analytes that contributed the most to PC1 in each region were all associated with salinity (Na, Cl, TS). This is expected for the Chesapeake soils where salinity is a strong factor in these estuarine water-adjacent ecosystems. In these sites, the marshes, which are closest to the estuary, have the highest concentrations of these analytes (Appendix A7).

The Erie soils had lower concentrations of Na, Cl, TS, but these analytes still followed similar ordering by transect position: upland < transition < marsh. In the Lake Erie region, fluvial sources (rivers) have higher salinity than the lake (Baker et al., 2014; Kane et al., 2022; Krieger, 2003) which would make a reverse gradient from the saline dominated Chesapeake perhaps more logical (i.e., upland > transition > marsh). The observed gradient in Erie soils may therefore reflect inputs from terrestrial sources that feed into rivers; the Erie sites also have sulfate in groundwater (Howard & Lopez, 2019; Michalovicz et al., 2002), so the higher concentrations in marshes may reflect greater groundwater influence. The salts may further be leached from the upland soils and retained in the marshes because of higher cation and anion exchange capacity (see Appendix A7).

The statistically important analytes for each region (Figure 4; Ca, Fe, NH_4-N for Erie and Al, P for Chesapeake) generally represented the parent material and environment, which influences soil development. The carbonate bedrock in Erie is a strong source of Ca while the high muscovite content in Chesapeake contributes to Al (Appendix A7). Agricultural activities and relatively high atmospheric N-deposition rates in the western Lake Erie basin may also be associated with the high NH_4-N concentrations in these soils (Choquette et al., 2019; Knorr et al., 2023; NADP, 2022).

We emphasize that these analytes are *strong contributors of variability* in our data and may not have a commensurate ecological or biogeochemical relevance to the systems. For instance, an analyte such as P may be highly relevant in the Erie region because of agricultural inputs (Maccoux et al., 2016; Ohio, 2016), but P is not a strong source of variability observed among our Erie samples. In contrast, the lower P values in Chesapeake coupled with high variability make it a stronger source of overall variability in the Chesapeake soils. Overall, our results provide support for our first hypothesis that freshwater and saltwater environments have variable sources of soil biogeochemical properties.

4.3. Transitions as Soil Biogeochemical Hotspots

Our second hypothesis that transitional coastal soils would show properties intermediate between the upland and marsh was supported by analytes such as TS, Na, and Cl (Figure 5), but not others. In particular, WEOC, P, and Fe had non-monotonic trends.

High WEOC concentrations in the Erie transition soils may be due to increased tree die-off and a concurrent increased input of carbon-rich organic debris to transition zone soils, which then accumulates under flooded conditions (I. M. Smith et al., 2021; Theuerkauf & Braun, 2021). P retention in marsh areas has been shown to be primarily due to sedimentation and adsorption (Bridgham et al., 2001; Messina & Conner, 1997), and we suggest

that the bidirectional hydrodynamic flow in the transitional zone means that the large quantities of water-mobilized nutrients may move back and forth along the coastal transect. As a result, some of these nutrients may be precipitated or deposited in the transitional soils (i.e., the bathtub ring effect) (Bridgham et al., 2001). Our data are generally consistent with this hypothesis. For example, P retention is influenced by pH, Ca, SOM, and redox conditions (Carter et al., 2022; Gibbons & Bridgeman, 2020; Holford & Patrick, 1979; Sah & Mikkelsen, 1989) and the frequent redox fluctuations of these systems (Patel et al., 2024; Regier et al., 2023) may promote precipitation of poorly crystalline Fe-oxides with fresh surfaces for binding phosphate (Darke & Walbridge, 2000; Herndon et al., 2019).

In the Chesapeake soils, Fe peaked in the transition zone at concentrations 2–3× higher than the upland and marsh values (Figures 5 and 6). Fe is more soluble and therefore more mobile in anoxic marsh soils compared with oxic upland soils (Deng & Stumm, 1993; Lindsay, 1988). Iron cycling may be most dynamic in transition zones because redox shifts from water fluctuations cause Fe reductive dissolution with anaerobiosis and oxidation and precipitation of poorly crystalline Fe-oxides under oxic conditions (Ellery et al., 2024). There may also be Fe inputs from groundwater or estuarine water that oxidize and accumulate in the transition zone. These transition zones, where biogeochemical processes such as Fe cycling are particularly intensified, may function as biogeochemical control points—locations where the rates of such processes are disproportionately high relative to the surrounding environment (Bernhardt et al., 2017). Even though rates are not directly measured here, elevated concentrations of redox-sensitive analytes such as Fe, C, and P may serve as indicators of heightened biogeochemical activity, pointing to the likelihood of these zones functioning as hotspots. However, the inconsistency of these patterns between and within our study regions suggests that site-specific contributors remain important moderators of biogeochemical activity in transitional zones.

In the Chesapeake sites, NH_4-N values showed inconsistent trends. Ammonium retention is dependent on surface charge and is therefore highly influenced by SOM%, specific conductance, and CEC (Compton & Church, 2011); further complicating this is the conversion of NH_4-N to NO_3-N. The lack of clear trends makes it difficult to identify a common mechanism, but this highlights the need to further study retention and mobility of N across the TAI (Wilson & Megonigal, 2025).

4.4. Soil Analytes as Indicators of Ecosystem Change

Our transect design represents a space-for-time substitution along the coastal continuum, with the assumption that the transitional forests started as upland forests and are turning into marsh systems (Y. Chen & Kirwan, 2024). Thus, a transition soil that is more similar to the marshes than to uplands may indicate a system that is further along its conversion into a marsh. Similarly, our results can also provide insights into which soil analytes are most responsive to ecosystem change driven by sea or lake level rise. For instance, in Chesapeake soils, transition zone Na concentrations were numerically closer to the marsh than the upland with increasing estuarine salinity (GCW < MSM < GWI). Similar trends were observed with Ca, K, CEC, and TS (Figure 5, Appendix A7). This is not surprising because these are analytes commonly associated with seawater (Morcos, 1970), but we suggest that Ca, K, CEC, and TS could be used as key indicator analytes to track how salinity-stressed a system may be, or how "far along" the ecosystem is in its transition phase.

With intensifying sea level rise and frequent inundation, there are shifts in soil salinity and oxygen availability (Machado-Silva et al., 2024; Patel et al., 2024; Regier et al., 2025), which in turn influence biogeochemical transformations and nutrient availability, as seen in our results for C, P, and Fe. As marsh systems shift toward uplands, salinity and hypoxia precede plant stress, hydraulic failure, and tree death (McDowell et al., 2022), leading to ghost forest formation. While this forest retreat may occur on a decadal scale (Y. Chen & Kirwan, 2024), the belowground processes may occur at faster scales and could be considered precursors of tree mortality and ecosystem shifts. Thus, soil biogeochemical and physical responses may be more indicative of early ecosystem stress than aboveground responses.

5. Synthesis and Modeling Implications

The physical, chemical, and biological complexity of coastal TAIs makes them challenging to model, which is necessary to gain predictive understanding of how such systems respond to environmental disturbances and other ecosystem change (Li et al., 2024; O'Meara et al., 2024; Sulman et al., 2024; Ward et al., 2020). Efforts to characterize the entire TAI are rare (Craft, 2012; Krauss et al., 2009), as most studies focus either on the terrestrial

Table 3
Priority Analytes Identified in This Paper as Sources of Variability in Coastal Soil Biogeochemistry

Analyte	Reason for priority	Region of importance
Fe	Strong contributor to regional variability	Erie
	Non-linear trends along the TAI	Chesapeake
P	Strong contributor to regional variability	Chesapeake
	Non-linear trends along the TAI	Erie
WEOC	Non-linear trends along the TAI	Erie
NH_4-N	Non-linear trends along the TAI	Chesapeake
Al	Strong contributor to regional variability	Chesapeake

Note. We prioritize analytes that contribute to variability across regions (Lake Erie and Chesapeake Bay), or across coastal terrestrial-aquatic interface (TAI) gradients (upland, transition, and marsh).

upland systems or the marsh systems, but not their interface (Golaz et al., 2019; Sengupta et al., 2021; US-DOE, 2017; Yu et al., 2021). Transition zones are not simply upland forests that are wet; they represent a unique position along the coastal TAI with distinct biogeochemical patterns and sources of variability. It is the evolution of these transition zones that will help us better understand ghost forest biogeochemistry and inland marsh migration. Model representation of the transition zones can also improve predictions of how upland ecosystem processes may change in the future (Li et al., 2024). To better understand coastal TAI soils, we need to know where on the landscape to focus measurements and which soil analytes and processes to represent in biogeochemical models (O'Meara et al., 2024; Sulman et al., 2024).

Our results allow us to identify priority analytes based on two criteria: (a) unique analytes that contribute strongly to variability in a given region (Figure 4), and (b) analytes that show unexpected or unpredictable trends along the TAI (Figure 5).

Identifying unique sources of variability in soils allows us to identify key parameters that may be transferable across different coastal systems; analytes such as Na, Cl, TS might be important parameters for any coastal system. Transferable sources of variability may indicate common underlying processes across sites. In contrast, for variables that are more discriminatory between regions, we can determine which variables are most important for a given region. Hence, an analyte such as extractable Al, which was below-detection in most of the Erie soils, may be less important for Erie coastal systems, but would need to be measured for the Chesapeake. Using such a framework, we can identify priority variables instead of employing a broad-spectrum "measure everything" approach.

Similarly, analytes such as Na, Cl, S may be easily modeled for these systems, as they follow linear and expected trends along the TAI. In contrast, analytes such as Fe, P, C, NH_4-N, which do not follow clean trends, may need more investigation and mechanistic understanding.

Based on our results, we suggest that C, Fe, Al and P are the most important elements to measure across upland-to-marsh and fresh-to-saline coastal gradients (Table 3). A deeper investigation into these elements will improve our understanding of biogeochemical cycling in the Chesapeake Bay and Lake Erie coastal regions and improve our ability to model how these elements cycle in coastal regions. These three analytes may not be consistently relevant across all ecosystems/regions, but we suggest that data-driven approaches, such as that used here, may rapidly generate new mechanistic hypotheses and understanding of ecosystem dynamics. Our region-level inferences are based on small sample size, so we need to be cautious when interpreting our results. However, related distributed networks (Myers-Pigg et al., 2023) could be leveraged to cover a larger spatial area while targeting these priority analytes. Future investigations of investigations of seasonal variability in coastal soils could also use our results and to prioritize target analytes. We especially expect redox-related analytes to vary significantly between dry and wet seasons, particularly in the transitions and marshes where ground water redox potential fluctuates seasonally (Machado-Silva et al., 2024).

It will be crucial to test such hypotheses through numerical modeling to complement experimental and observational studies. Only through such combined model-experimental workflows and analyses (Hanson & Walker, 2020) will we be able to fundamentally improve the predictability of the complex and crucial ecosystems at the terrestrial-aquatic interface.

Appendix A: Additional Characterization of the Sites

A1. Hydrologic Characteristics of the Sites

Soil water content was measured using TEROS 12 moisture sensor (Meter Group) at a 10-cm depth for the period January-December 2023. Water level was measured using Aqua TROLL 600 Multiparameter Sondes (In situ Inc.) during this period. A positive value of water level indicates water was above ground surface (i.e., site was flooded), a negative value indicated water was below ground surface. Water level data are not available for GCW upland and for OWC upland/transition.

Journal of Geophysical Research: Biogeosciences

10.1029/2025JG008978

	Erie								
	Crane Creek (CRC)			Portage River (PTR)			Old Woman Creek (OWC)		
	Upland	Transition	Marsh	Upland	Transition	Marsh	Upland	Transition	Marsh
Mean annual soil water content (% v/v)	33.14 ± 5.82	44.25 ± 4.18	52.61 ± 1.79	29.79 ± 6.92	31.53 ± 7.58	49.54 ± 4.25	34.01 ± 1.59	44.08 ± 2.79	49.25 ± 1.78
Mean annual water level (m)	(−) 3.06 ± 1.07	complete annual record not available	(−) 0.02 ± 0.10	(−) 2.19 ± 1.33	complete annual record not available	(−) 0.28 ± 0.10	no sensor at this location	complete annual record not available	(+) 0.03 ± 0.12
Time flooded (% of year)	0		57.96	0		0.19			25.68
	Chesapeake								
	Global Change Research Wetland (GCW)			Moneystump Marsh (MSM)			Goodwin Islands (GWI)		
	Upland	Transition	Marsh	Upland	Transition	Marsh	Upland	Transition	Marsh
Mean annual soil water content (% v/v)	no sensor at this location	48.29 ± 3.90	59.52 ± 1.32	38.46 ± 5.47	52.90 ± 4.65	62.78 ± 0.79	30.26 ± 3.36	55.01 ± 2.97	61.97 ± 0.89
Mean annual water level (m)	(−) 4.08 ± 0.25	(−) 0.46 ± 0.06	(−) 0.09 ± 0.07	(−) 0.29 ± 0.22	(−) 0.08 ± 0.05	(−) 0.08 ± 0.09	(−) 0.50 ± 0.14	(−) 0.15 ± 0.08	(−) 0.04 ± 0.07
Time flooded (% of year)	0	0	7.77	1.38	3.90	12.97	0.02	0.88	8.08

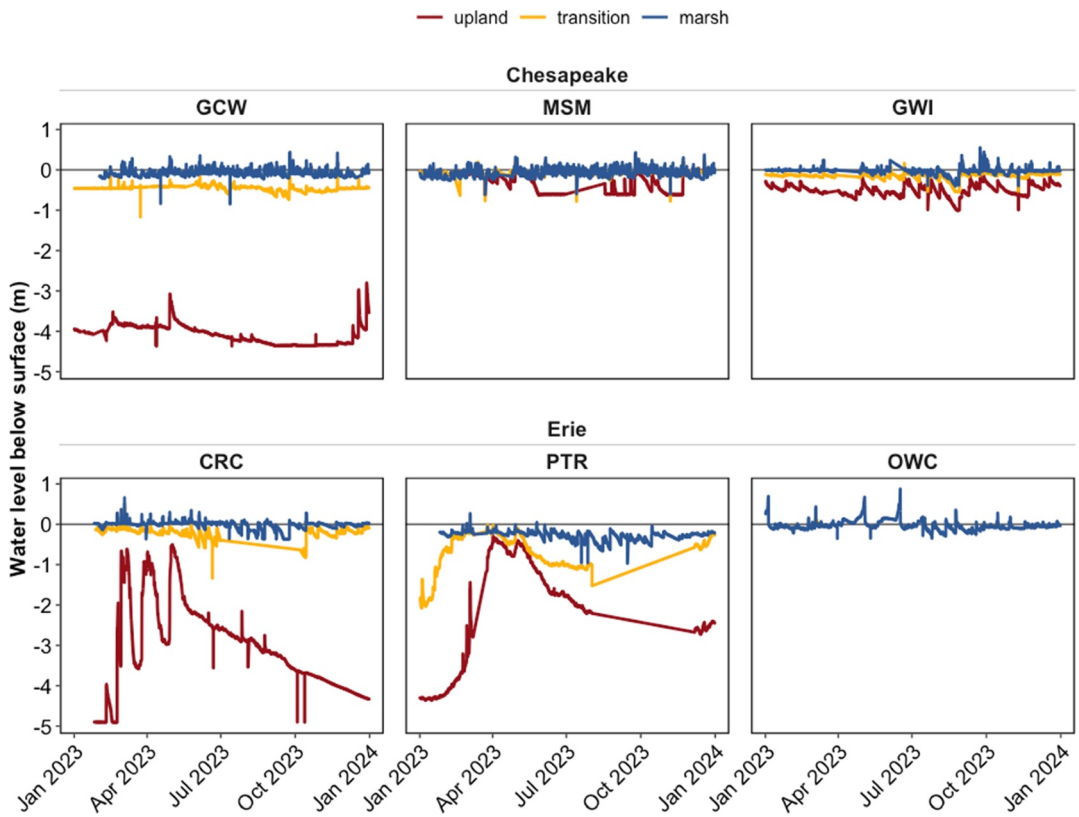

Soil water level for January-December 2023: Water level was measured using Aqua TROLL 600 Multiparameter Sondes. Negative values indicate water level below the surface, positive values indicate water level above the surface, that is, the soils were inundated. Data are not available for GCW upland and for OWC upland/transition.

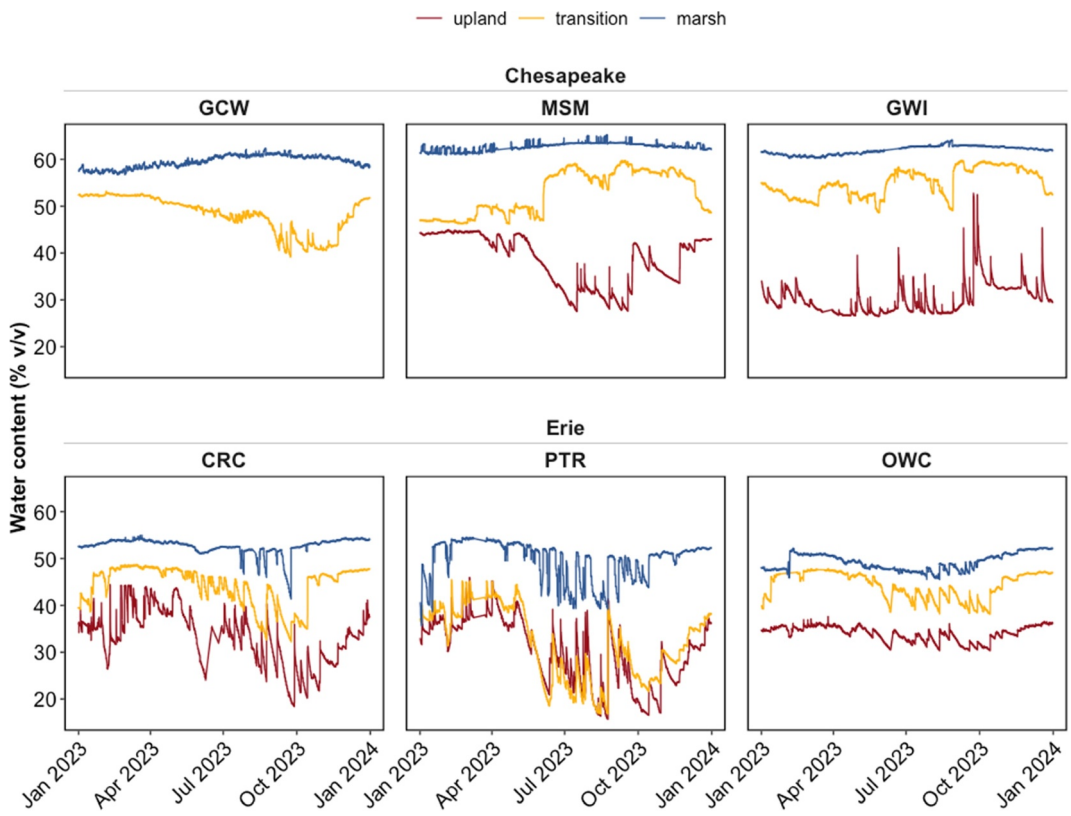

Soil water content for January-December 2023: Volumetric water content was measured using TEROS 12 moisture sensor (Meter Group) at a 10-cm depth. Data are not available for GCW upland.

A2. List of Analyses Included in This Study

Summary of chemical analyses performed and included in this study.

Analyte	Analyte category	Measurement
Grab samples—freeze-dried samples		
TC (total carbon)	Bulk chemistry	Catalytic combustion
TN (total nitrogen)		Catalytic combustion
TS (total sulfur)		Catalytic combustion
SOM (soil organic matter)		Loss on ignition
pH		pH/SC meter
Specific Conductance		pH/SC meter
Grab samples—field moist samples		
WSOC	Water-extractable carbon	Catalytic combustion
WSIC		Catalytic combustion
NH_4-N (extractable ammonium)	Extractable nutrients	Colorimetric analysis
NO_3-N (extractable nitrate)		Colorimetric analysis
P (extractable phosphorus)		Mehlich-III extraction, colorimetric analysis
Fe (extractable, poorly crystalline iron)		HCl extraction, ferrozine colorimetric method

Table
Continued

Analyte	Analyte category	Measurement
Ca (calcium)	Salt-extractable cations	1M NH4Cl extraction, ICP-OES
Mg (magnesium)		1M NH4Cl extraction, ICP-OES
Na (sodium)		1M NH4Cl extraction, ICP-OES
K (potassium)		1M NH4Cl extraction, ICP-OES
Al (aluminum)		1M NH4Cl extraction, ICP-OES
CEC (cation exchange capacity)		Calculated index; sum of all extractable cations
SO_4 (sulfate)	Water-extractable anions	Ion chromatography
Cl (chloride)		Ion chromatography

Summary of physical analyses performed.

Analyte	Measurement
Intact soil cores	
Bulk density	Bulk density ring
Water retention curves	HYPROP + WP4C devices
Grab samples—oven/freeze-dried	
Texture	Hydrometer
Particle density	Pycnometer
Mineralogy	X-ray diffraction

A3. Correlations Among Measured Analytes

Correlation matrix for all analytes measured in this study. Green boxes represent significant positive correlations, orange boxes represent significant negative correlations, and blank boxes represent correlations that were non-significant ($p > 0.05$). Correlation coefficient (R) is denoted for each comparison. We used a cutoff of $R \geq 0.8$ to indicate highly correlated variables.

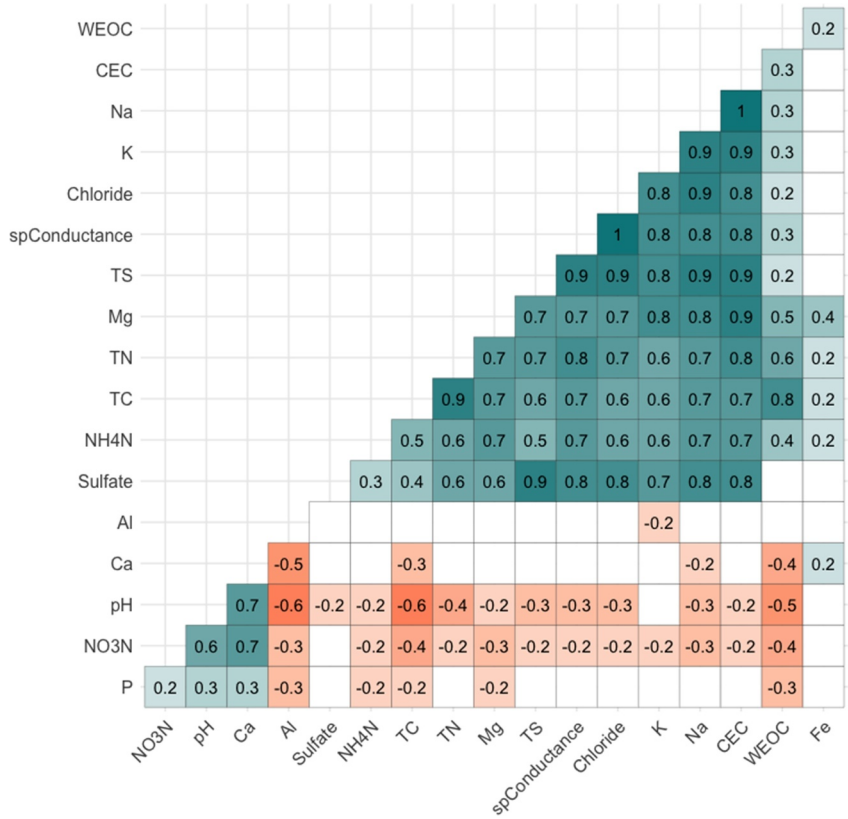

A4. Slopes/Elevation

CRC is a unique site with a discontinuous transect, where the upland forest location is on one side of the river, and the transition/marsh locations are on the other side. All of the other sites had linear transects. This decision was made because there were no "truly upland" areas in the marsh/transition containing plot; all trees in the transition already showed signs of stress. Thus, we selected an unstressed upland forest nearby (~1 km away).

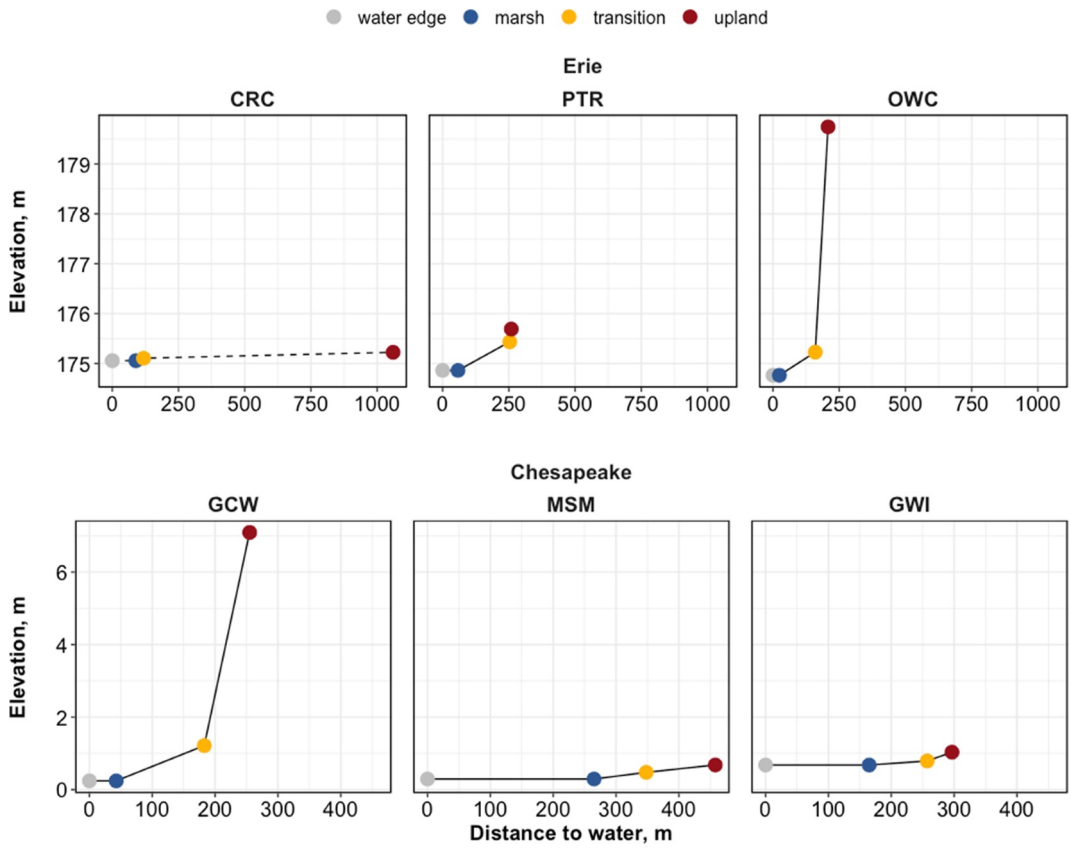

A5. Water Retention Curves

Curves were fitted using the Van Genuchten equation, the fitted model parameters are provided below.

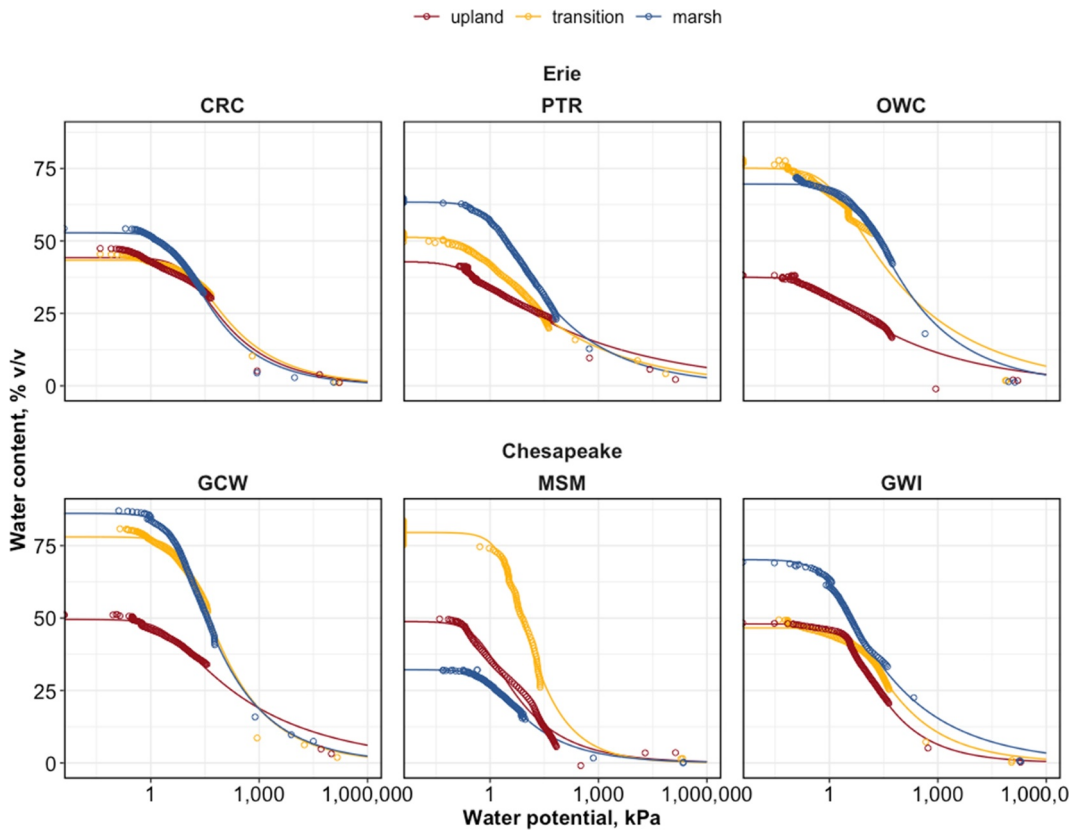

α is a scale parameter that is inversely proportional to the mean pore diameter, n is a shape parameter that controls the slope of the soil-water characteristic curve, θ_r is the residual water content, and θ_s is the saturated water content.

	CRC			PTR			OWC		
	Upland	Transition	Marsh	Upland	Transition	Marsh	Upland	Transition	Marsh
α	0.00903	0.00648	0.0176	0.4057	0.1482	0.0737	0.2344	0.115	0.0141
n	1.299	1.294	1.315	1.121	1.188	1.231	1.154	1.147	1.247
θ_r	0	0	0	0	0	0	0	0	0
θ_s	0.443	0.434	0.531	0.416	0.495	0.634	0.375	0.755	0.696

	GCW			MSM			GWI		
	Upland	Transition	Marsh	Upland	Transition	Marsh	Upland	Transition	Marsh
α	0.0427	0.00871	0.0163	0.1691	0.0279	0.0926	0.1135	0.0129	0.0239
n	1.153	1.319	1.3	1.33	1.482	1.331	1.214	1.313	1.368
θ_r	0	0	0	0	0	0	0	0	0
θ_s	0.497	0.78	0.861	0.488	0.795	0.322	0.697	0.465	0.48

A6. GWI Case Study

The sites in each region were chosen to capture geological and/or biogeochemical gradients while zones within transects were chosen based on a visual assessment of forest condition to include healthy trees (upland), stressed

trees (transition), and tree absence (marsh). We could not control for other macroscale and microscale factors such as slope, distance to water, tidal range, microtopography, and local hydrology that are required to explain some of the patterns in our data.

For example, the GWI site is located in the highest salinity part of the Bay among our Chesapeake sites (~25 psu) yet had marsh samples with very low specific conductance (<100 µS/cm) and chloride (2.77 meq/100 g) values. Similarly, specific conductance in GCW transition samples were near zero, showing no evidence of seawater exposure. In both cases, the most likely explanation is dilution by fresh groundwater discharge, which is consistent with the fact that these zones are located a large distance (~200 m) from the estuary and therefore relatively uncoupled from tidal flooding. These examples highlight the importance of geomorphology and groundwater hydrology in regulating both microscale and macroscale variation that is crucial to capture for spatiotemporal scaling and modeling.

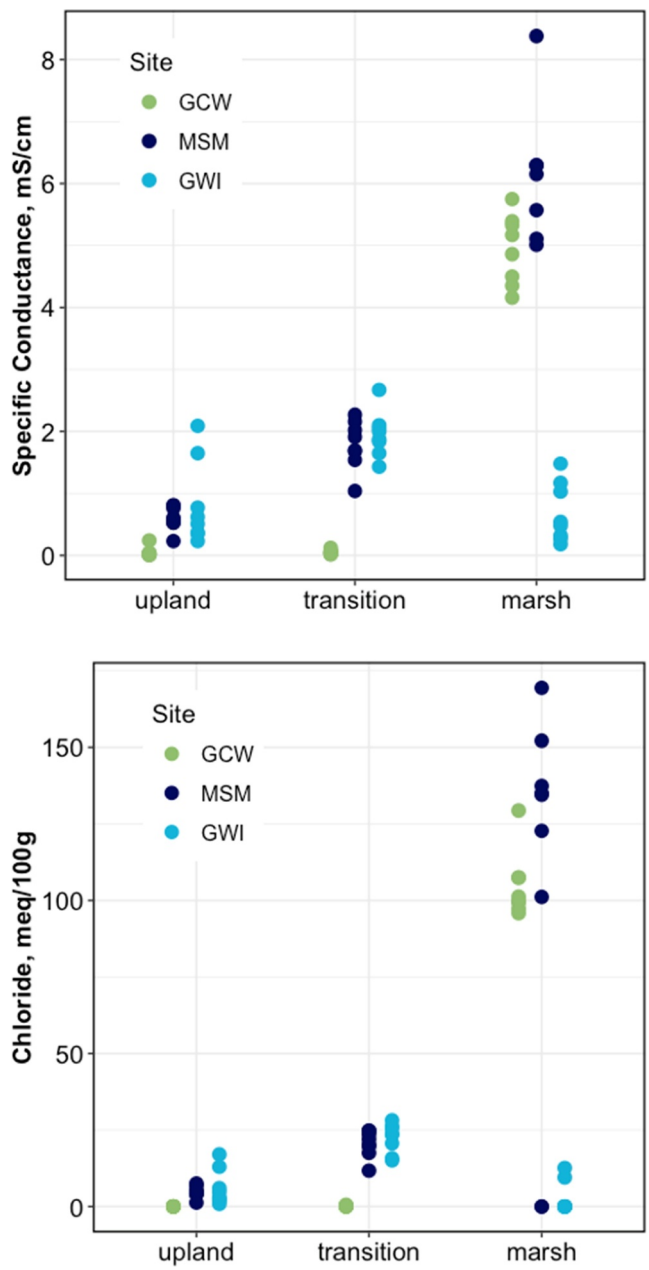

A7. Summary Tables of Chemical Analytes Included in the Analysis

Summary of bulk soil analytes: Data are presented as mean ± standard error for each site, followed by a mean across all sites for the given transect position (highlighted in gray). Different lower-case letters denote statistically significant differences among sites for a given transect position. Different upper-case letters denote statistically significant differences among transect positions for a given region. Different Greek letters denote significant differences among transect positions for a given site.

		Erie				Chesapeake		
		Upland	Transition	Marsh		Upland	Transition	Marsh
Total C, %	CRC	7.14 ± 0.42 *a β*	12.02 ± 0.96 *a α*	7.66 ± 0.33 *a β*	GCW	4.22 ± 0.48 *b ψ*	7.63 ± 0.76 *b β*	30.76 ± 0.81 *a α*
	PTR	7.27 ± 0.26 *a α*	10.08 ± 1.87 *ab α*	7.71 ± 0.25 *a α*	MSM	32.64 ± 1.09 *a α*	29.67 ± 1.33 *a α*	32.86 ± 2.1 *a α*
	OWC	5.11 ± 0.39 *b α*	6.48 ± 0.46 *b α*	6.5 ± 0.58 *a α*	GWI	32.26 ± 1.67 *a α*	26.27 ± 1.53 *a α*	14.51 ± 2.83 *b β*
	Mean	6.51 ± 0.28 *B*	9.64 ± 0.84 *A*	7.39 ± 0.22 *B*	Mean	23.04 ± 2.85 *A*	20 ± 2.42 *A*	26.13 ± 2.1 *A*
Total N, %	CRC	0.52 ± 0.03 *a β*	0.83 ± 0.05 *a α*	0.73 ± 0.04 *a α*	GCW	0.23 ± 0.03 *b ψ*	0.41 ± 0.04 *c β*	1.61 ± 0.02 *a α*
	PTR	0.57 ± 0.02 *a α*	0.81 ± 0.15 *a α*	0.68 ± 0.02 *a α*	MSM	1.13 ± 0.07 *a β*	1.52 ± 0.08 *a α*	1.71 ± 0.09 *a α*
	OWC	0.36 ± 0.02 *b β*	0.45 ± 0.03 *b αβ*	0.51 ± 0.04 *b α*	GWI	1.26 ± 0.07 *a α*	1.22 ± 0.07 *b α*	0.73 ± 0.13 *b β*
	Mean	0.48 ± 0.02 *B*	0.71 ± 0.06 *A*	0.65 ± 0.02 *A*	Mean	0.87 ± 0.1 *B*	1 ± 0.12 *B*	1.35 ± 0.11 *A*
Total S, %	CRC	0.05 ± 0 *a* ψ	0.15 ± 0.01 *a β*	0.21 ± 0.03 *a α*	GCW	0.02 ± 0 *b β*	0.06 ± 0.01 *c β*	1.84 ± 0.08 *a α*
	PTR	0.06 ± 0 *a β*	0.09 ± 0.02 *b αβ*	0.13 ± 0.01 *b α*	MSM	0.19 ± 0.05 *a β*	0.43 ± 0.06 *a β*	1.74 ± 0.13 *a α*
	OWC	0.03 ± 0 *b β*	0.04 ± 0 *c β*	0.09 ± 0.01 *b α*	GWI	0.15 ± 0.01 *a β*	0.27 ± 0.02 *b αβ*	0.4 ± 0.08 *b α*
	Mean	0.05 ± 0 C	0.09 ± 0.01 *B*	0.14 ± 0.01 *A*	Mean	0.12 ± 0.02 *B*	0.22 ± 0.04 *B*	1.32 ± 0.15 *A*
pH	CRC	6.71 ± 0.06 *a α*	6.51 ± 0.11 *ab α*	6.72 ± 0.15 *a α*	GCW	5.22 ± 0.13 *a α*	4.6 ± 0.07 *c β*	5.5 ± 0.06 *a α*
	PTR	6.01 ± 0.15 *b α*	6.03 ± 0.26 *b α*	6.57 ± 0.16 *a α*	MSM	4.16 ± 0.08 *b β*	5.18 ± 0.16 *b α*	4.72 ± 0.23 *b αβ*
	OWC	6.2 ± 0.18 *b β*	6.97 ± 0.1 *a α*	6.36 ± 0.1 *a β*	GWI	4.61 ± 0.17 *b ψ*	6.55 ± 0.05 *a α*	5.92 ± 0.1 *a β*
	Mean	6.31 ± 0.1 *A*	6.5 ± 0.12 *A*	6.56 ± 0.09 *A*	Mean	4.67 ± 0.12 *B*	5.44 ± 0.18 *A*	5.36 ± 0.13 *A*
Specific Conductance, mS/cm	CRC	0.11 ± 0 a*b β*	0.2 ± 0.02 *a β*	0.63 ± 0.11 *a α*	GCW	0.05 ± 0.03 *b β*	0.05 ± 0.01 *b β*	4.94 ± 0.2 *b α*
	PTR	0.12 ± 0.01 *a β*	0.2 ± 0.09 *a αβ*	0.34 ± 0.04 *b α*	MSM	0.61 ± 0.07 *a* ψ	1.79 ± 0.14 *a β*	6.12 ± 0.43 *a α*
	OWC	0.08 ± 0.01 *b β*	0.08 ± 0.01 *a β*	0.19 ± 0.02 *b α*	GWI	0.82 ± 0.24 *a β*	1.95 ± 0.13 *a α*	0.68 ± 0.17 *c β*
	Mean	0.1 ± 0.01 *B*	0.16 ± 0.03 *B*	0.39 ± 0.05 *A*	Mean	0.49 ± 0.1 *B*	1.26 ± 0.19 *B*	3.82 ± 0.52 *A*
% OM	CRC	15.01 ± 0.82 *a β*	24.82 ± 2.15 *a α*	15.6 ± 1.05 *a β*	GCW	7.7 ± 0.91 *b ψ*	14.04 ± 1.15 *c β*	66.41 ± 1.39 *a α*
	PTR	15.05 ± 0.51 *a α*	21.14 ± 4.14 *a α*	17.26 ± 0.54 *a α*	MSM	73.29 ± 4.89 *a α*	75.59 ± 1.68 *a α*	70.12 ± 2.04 *a α*
	OWC	10.89 ± 0.76 *b α*	15.44 ± 2.21 *a α*		GWI	64.23 ± 4.09 *a α*	62.47 ± 3.02 *b α*	26.38 ± 4.48 *b β*
	Mean	13.65 ± 0.55 *B*	20.47 ± 1.82 *A*	16.64 ± 0.53 *B*	Mean	48.41 ± 6.39 *A*	50.7 ± 5.64 *A*	54.94 ± 4.32 *A*

Summary of salt-extractable cations: Data are presented as mean ± standard error for each site, followed by a mean across all sites for the given transect position (highlighted in gray). Different lower-case letters denote statistically significant differences among sites for a given transect position. Different upper-case letters denote statistically significant differences among transect positions for a given region. Different Greek letters denote significant differences among transect positions for a given site.

		Erie				Chesapeake		
		Upland	Transition	Marsh		Upland	Transition	Marsh
Al (meq/100 g)	CRC	0 *a α*	0 *a α*	0 *a α*	GCW	1.63 ± 0.77 a*b β*	4.01 ± 0.77 *a α*	0.06 ± 0.03 *a β*
	PTR	0.02 ± 0 *a α*	0.04 ± 0.03 *a α*	0 *a α*	MSM	2.59 ± 0.25 *a α*	0.44 ± 0.24 *b β*	0.26 ± 0.15 *a β*
	OWC	0.03 ± 0.03 *a α*	0 *a α*	0 *a α*	GWI	0.61 ± 0.17 *b α*	0.02 ± 0.01 *b β*	0.08 ± 0.03 *a β*
	Mean	0.02 ± 0.01 *A*	0.02 ± 0.01 *A*	0 *A*	Mean	1.61 ± 0.31 *B*	1.49 ± 0.45 *B*	0.14 ± 0.06 *A*
Ca (meq/100g)	CRC	9.63 ± 0.41 *a β*	15.4 ± 1.09 *a α*	17.12 ± 1.71 *a α*	GCW	3.84 ± 0.58 *a β*	1.02 ± 0.1 *c* ψ	8.76 ± 0.45 *a α*
	PTR	8.67 ± 0.21 *a* ψ	10.82 ± 0.77 *b β*	14 ± 0.49 *a α*	MSM	1.38 ± 0.2 *b β*	4.97 ± 0.56 *b α*	5.01 ± 0.48 *b α*
	OWC	5.33 ± 0.46 *b β*	8.86 ± 0.58 *b α*	9.17 ± 0.97 *b α*	GWI	3.01 ± 0.19 *a β*	9.26 ± 0.34 *a α*	3.21 ± 0.46 *c β*
	Mean	7.88 ± 0.42 C	11.69 ± 0.71 *B*	13.67 ± 0.77 *A*	Mean	2.74 ± 0.29 *B*	5.08 ± 0.73 *A*	5.5 ± 0.53 *A*
K (meq/100g)	CRC	0.81 ± 0.06 *b α*	0.52 ± 0.06 *a β*	0.48 ± 0.07 a*b β*	GCW	0.56 ± 0.07 *b β*	0.48 ± 0.04 *c β*	2.77 ± 0.15 *a α*
	PTR	1.12 ± 0.09 *a α*	1.04 ± 0.24 *a αβ*	0.58 ± 0.08 *a β*	MSM	0.48 ± 0.06 *b β*	0.73 ± 0.07 *b β*	2.87 ± 0.23 *a α*
	OWC	0.77 ± 0.05 *b α*	0.73 ± 0.16 *a α*	0.2 ± 0.02 *b β*	GWI	1.05 ± 0.08 *a β*	2.14 ± 0.08 *a α*	1.68 ± 0.26 *b α*
	Mean	0.9 ± 0.05 *B*	0.76 ± 0.1 *B*	0.46 ± 0.05 *A*	Mean	0.7 ± 0.07 C	1.12 ± 0.16 *B*	2.44 ± 0.17 *A*
Mg (meq/100g)	CRC	3.62 ± 0.12 *a β*	5.55 ± 0.35 *a α*	4.68 ± 0.29 *b α*	GCW	2.53 ± 0.46 *a β*	2.32 ± 0.21 *c β*	32.56 ± 0.81 *a α*
	PTR	2.3 ± 0.16 *b* ψ	3.47 ± 0.37 *b β*	5.9 ± 0.29 *a α*	MSM	8.47 ± 4.4 *a β*	17.02 ± 2.03 *b αβ*	24.85 ± 2.49 *a α*
	OWC	1.94 ± 0.13 *b β*	3.18 ± 0.43 *b α*	2.87 ± 0.26 *c αβ*	GWI	8.98 ± 0.67 *a β*	35.19 ± 1.33 *a α*	14.81 ± 2.45 *b β*
	Mean	2.62 ± 0.16 C	4.07 ± 0.3 *B*	4.8 ± 0.28 *A*	Mean	6.66 ± 1.55 *B*	18.18 ± 2.91 *A*	23.75 ± 1.91 *A*
Na (meq/100g)	CRC	0.05 ± 0.01 *a β*	0.34 ± 0.05 *a α*	0.38 ± 0.03 *a α*	GCW	0.04 ± 0 *c β*	0.49 ± 0.16 *c β*	81.46 ± 4.01 *a α*
	PTR	0.06 ± 0.01 *a* ψ	0.16 ± 0.02 *b β*	0.38 ± 0.02 *a α*	MSM	5.93 ± 0.44 *b β*	18.75 ± 0.79 *b β*	95.73 ± 9.81 *a α*
	OWC	0.03 ± 0 *b* ψ	0.09 ± 0.01 *b β*	0.2 ± 0.01 *b α*	GWI	14.78 ± 1.45 *a β*	39.72 ± 1.24 *a α*	47.38 ± 9.84 *b α*
	Mean	0.05 ± 0 C	0.19 ± 0.03 *B*	0.34 ± 0.02 *A*	Mean	6.92 ± 1.35 C	19.65 ± 3.37 *B*	75.45 ± 6.5 *A*
CEC (meq/100g)	CRC	14.11 ± 0.46 *a β*	21.8 ± 1.38 *a α*	22.67 ± 1.93 *a α*	GCW	8.61 ± 1.08 *b β*	8.32 ± 0.64 *c β*	125.6 ± 4.49 *a α*
	PTR	12.17 ± 0.17 *b* ψ	15.53 ± 1.06 *b β*	20.86 ± 0.61 *a α*	MSM	18.85 ± 4.54 a*b β*	41.92 ± 2.92 *b β*	128.72 ± 12.77 *a α*
	OWC	8.1 ± 0.58 *c β*	12.87 ± 0.58 *b α*	12.44 ± 1.24 *b α*	GWI	28.43 ± 2.31 *a β*	86.31 ± 2.66 *a α*	67.16 ± 12.9 *b α*
	Mean	11.46 ± 0.55 C	16.73 ± 0.94 *B*	19.26 ± 0.98 *A*	Mean	18.63 ± 2.37 C	45.52 ± 6.78 *B*	107.29 ± 8.65 *A*

Summary of water-extractable anions: Data are presented as mean ± standard error for each site, followed by a mean across all sites for the given transect position (highlighted in gray). Different lower-case letters denote statistically significant differences among sites for a given transect position. Different upper-case letters denote statistically significant differences among transect positions for a given region. Different Greek letters denote significant differences among transect positions for a given site.

		Erie				Chesapeake		
		Upland	Transition	Marsh		Upland	Transition	Marsh
Chloride (meq/100 g)	CRC	0.01 ± 0 *a* ψ	0.27 ± 0.04 *a α*	0.17 ± 0.03 *a β*	GCW	0.02 ± 0 *b β*	0.15 ± 0.07 *b β*	104.7 ± 3.83 *a α*
	PTR	0.01 ± 0 *a* ψ	0.09 ± 0.02 *b β*	0.19 ± 0.02 *a α*	MSM	4.83 ± 0.67 *a β*	20.55 ± 1.55 *a β*	105.8 ± 20.94 *a α*
	OWC	0 ± 0 *a* ψ	0.03 ± 0.01 *b β*	0.07 ± 0.01 *b α*	GWI	6.13 ± 2.06 *a β*	22.34 ± 1.7 *a α*	2.77 ± 1.83 *b β*
	Mean	0.01 ± 0 *B*	0.13 ± 0.02 *A*	0.15 ± 0.02 *A*	Mean	3.66 ± 0.88 *B*	14.35 ± 2.22 *B*	72.48 ± 12.23 *A*
Sulfate (meq/100 g)	CRC	0.04 ± 0 a*b β*	0.64 ± 0.21 *a β*	6.66 ± 0.93 *a α*	GCW	0.01 ± 0 *b β*	0.13 ± 0.03 *b β*	42.56 ± 4.45 *a α*
	PTR	0.05 ± 0.01 *a β*	0.14 ± 0.03 *b β*	2.67 ± 0.67 *b α*	MSM	0.28 ± 0.03 a*b β*	2.17 ± 0.16 *a β*	24.04 ± 2.25 *b α*
	OWC	0.03 ± 0 *b β*	0.07 ± 0.01 *b β*	1.87 ± 0.21 *b α*	GWI	0.6 ± 0.2 *a β*	2.07 ± 0.17 *a β*	5.98 ± 1.69 *c α*
	Mean	0.04 ± 0 *B*	0.28 ± 0.08 *B*	3.59 ± 0.53 *A*	Mean	0.3 ± 0.08 *B*	1.46 ± 0.21 *B*	24.19 ± 3.41 *A*

Summary of other extractable nutrients: Data are presented as mean ± standard error for each site, followed by a mean across all sites for the given transect position (highlighted in gray). Different lower-case letters denote statistically significant differences among sites for a given transect position. Different upper-case letters denote statistically significant differences among transect positions for a given region. Different Greek letters denote significant differences among transect positions for a given site.

		Erie				Chesapeake		
		Upland	Transition	Marsh		Upland	Transition	Marsh
P (μg/g)	CRC	42.06 ± 20.21 *b αβ*	19.21 ± 2.42 *b β*	98.89 ± 27.71 *a α*	GCW	4.7 ± 0.65 *b β*	5.21 ± 0.83 *b β*	78.17 ± 23.41 *a α*
	PTR	204.26 ± 13.9 *a α*	256.48 ± 58.33 *a α*	58.02 ± 12.19 *a β*	MSM	3.54 ± 0.85 *b β*	6.24 ± 1.05 *b β*	42.88 ± 9.42 *ab α*
	OWC	20.92 ± 4.11 *b ψ*	160.87 ± 17.34 *a α*	109.85 ± 9.38 *a β*	GWI	29.24 ± 8.79 *a α*	11.74 ± 1.58 *a α*	21.4 ± 3.92 *b α*
	Mean	74.68 ± 17.69 *B*	145.52 ± 27.31 *A*	82.47 ± 10.47 *B*	Mean	12.88 ± 3.89 *B*	7.73 ± 0.89 *B*	47.3 ± 9.23 *A*
Fe (μg/g)	CRC	70.17 ± 5.16 *a β*	125.33 ± 20.61 *a β*	217.76 ± 31.3 *ab α*	GCW	27.02 ± 8.15 *b β*	160.38 ± 55.32 *b α*	71.78 ± 18.88 *a αβ*
	PTR	44.43 ± 3.99 *b β*	100.32 ± 12.53 *a β*	239.89 ± 18.87 *a α*	MSM	206.15 ± 48.38 *a αβ*	314.44 ± 38.4 *ab α*	105.57 ± 51.87 *a β*
	OWC	22.35 ± 2 *c β*	96.64 ± 14.37 *a α*	130.98 ± 8.39 *b α*	GWI	40.55 ± 18.91 *b β*	488.66 ± 82.05 *a α*	84.22 ± 22.21 *a β*
	Mean	45.65 ± 4.41 C	107.43 ± 9.33 *B*	208.58 ± 14.78 *A*	Mean	86.24 ± 22.99 *B*	313.88 ± 43.08 *A*	89.33 ± 21.62 *B*
NH_4-N (μg/g)	CRC	13.11 ± 0.41 *a β*	21.67 ± 0.92 *a α*	23.88 ± 2.69 *a α*	GCW	23.04 ± 1.16 *b α*	10.04 ± 3.79 *b β*	24.9 ± 3.61 *b α*
	PTR	11.42 ± 0.44 *a β*	16.3 ± 2.5 *ab β*	25.07 ± 1.75 *a α*	MSM	35.77 ± 2.64 *a β*	76.28 ± 11.55 *a αβ*	162.03 ± 47.19 *a α*
	OWC	12.76 ± 0.85 *a β*	13.82 ± 0.7 *b β*	18.96 ± 0.89 *a α*	GWI	22.94 ± 2.01 *b β*	94.56 ± 9.2 *a α*	37.95 ± 6.01 *b β*
	Mean	12.43 ± 0.36 C	17.26 ± 1.09 *B*	23.21 ± 1.19 *A*	Mean	27.25 ± 1.68 *B*	60.29 ± 8.99 *AB*	78.44 ± 20.9 *A*
NO_3-N (μg/g)	CRC	67.73 ± 3.54 *a α*	81.33 ± 17.59 *a α*	89.41 ± 23.97 *a α*	GCW	0.74 ± 0.02 *c ψ*	0.94 ± 0.06 *b β*	4.82 ± 0.07 *a α*
	PTR	62.81 ± 8.87 *a α*	104.64 ± 49.04 *a α*	89.92 ± 14.27 *a α*	MSM	2.3 ± 0.1 *a α*	3.39 ± 0.19 *a α*	11.56 ± 5.89 *a α*
	OWC	47.15 ± 6.61 *a α*	30.17 ± 6.1 *a αβ*	24.42 ± 3.98 *b β*	GWI	1.64 ± 0.14 *b β*	4.44 ± 0.96 *a α*	2.19 ± 0.31 *a β*
	Mean	59.23 ± 4.1 *A*	72.05 ± 17.87 *A*	73.4 ± 10.56 *A*	Mean	1.56 ± 0.14 *B*	2.92 ± 0.44 *AB*	6.4 ± 2.2 *A*

Summary of water-extractable forms of carbon: Data are presented as mean ± standard error for each site, followed by a mean across all sites for the given transect position (highlighted in gray). Different lower-case letters denote statistically significant differences among sites for a given transect position. Different upper-case letters denote statistically significant differences among transect positions for a given region. Different Greek letters denote significant differences among transect positions for a given site.

		Erie				Chesapeake		
		Upland	Transition	Marsh		Upland	Transition	Marsh
WEOC (μg/g)	CRC	59.99 ± 5.28 *a α*	74.44 ± 8.36 *a α*	65.89 ± 11.19 *a α*	GCW	51.39 ± 8.31 *b β*	81.12 ± 10.06 *b β*	186.51 ± 9.32 *b α*
	PTR	57.06 ± 12.28 *a α*	90.03 ± 27.16 *a α*	57.61 ± 5.78 *a α*	MSM	757.13 ± 46.66 *a α*	644.88 ± 38.71 *a α*	334.37 ± 28.22 *a β*
	OWC	69.42 ± 4.88 *a α*	78.73 ± 7.29 *a α*	49.48 ± 2.69 *a β*	GWI	790.88 ± 95.92 *a α*	631.41 ± 31.9 *a α*	296.25 ± 59.36 *ab β*
	Mean	62.16 ± 4.67 *AB*	81.07 ± 9.48 *A*	57.9 ± 4.21 *B*	Mean	533.13 ± 78.83 *B*	452.47 ± 57.14 *B*	274.86 ± 24.41 *A*
WEIC (μg/g)	CRC	5.17 ± 0.72 *a β*	33.32 ± 8.92 *a β*	127.33 ± 35.61 *a α*				
	PTR	2.1 ± 0.79 *b β*	5.32 ± 1.56 *b β*	92.44 ± 20.63 *ab α*	MSM	0 *α*	4.82 ± 4.4 *b α*	10.33 ± 8.58 *a α*
	OWC	6.2 ± 1.13 *a α*	24.06 ± 8.31 *ab α*	8.4 ± 3.18 *b α*	GWI	0 *β*	86.98 ± 18.55 *a α*	17.75 ± 5.12 *a β*
	Mean	4.42 ± 0.6 *B*	20.9 ± 4.55 *B*	81.24 ± 15.71 *A*	Mean	0 *B*	45.9 ± 14.05 *A*	13.82 ± 5.07 *B*

Summary of physical properties: Values are reported as percentage (mean ± se). Because soil texture is a property of the mineral soil fraction, it was not performed on highly organic samples (O horizons).

	CRC			PTR			OWC		
	Upland	Transition	Marsh	Upland	Transition	Marsh	Upland	Transition	Marsh
Bulk Density				0.87	0.39	0.29	0.87	0.71	0.4
Particle Density	2.7 ± 0.03	2.64 ± 0.06	1.92 ± 0.13	2.5 ± 0.03	2.35 ± 0.06	2.58 ± 0.05	2.45 ± 0.04	2.55 ± 0.01	2.34 ± 0.02
Texture									
Sand (%)	9.9 ± 1.92	9.44 ± 0.5	4.46 ± 0.58	14.37 ± 0.46	12.73 ± 1.26	6.02 ± 1.1	28.3 ± 1.64	10.69 ± 2.14	3.22 ± 0.28
Silt (%)	69.77 ± 6.02	79.7 ± 5.39	31.74 ± 4.62	83.53 ± 2.41	67.63 ± 9.15	49.08 ± 6.4	57.75 ± 6.82	77.53 ± 9.22	90.3 ± 5.71
Clay (%)	20.33 ± 4.16	10.87 ± 5.04	63.8 ± 4.61	2.1 ± 1.95	19.64 ± 8.02	44.9 ± 7.35	13.96 ± 7.95	11.79 ± 11.37	6.48 ± 5.99
Texture class	*Silt loam*	*Silt loam*	*Clay*	*Silt*	*Silt loam*	*Silty clay*	*Silt loam*	*Silt loam*	*Silt*

	GCW			MSM			GWI		
	Upland	Transition	Marsh	Upland	Transition	Marsh	Upland	Transition	Marsh
Bulk Density	0.77	0.38	0.24	0.15	0.16	0.1	0.42	1.01	1.49
Particle Density	2.47 ± 0.02	0.64 ± 0.05	–	0.26 ± 0	0.35 ± 0.03	–	2.31 ± 0.04	2.65 ± 0.07	–
Texture									
Sand (%)	47.27 ± 2.31	40.78 ± 9.31	–	–	–	–	–	–	–
Silt (%)	36.7 ± 3.6	32.16 ± 4.95	–	–	–	–	–	–	–
Clay (%)	16.04 ± 2.41	27.07 ± 4.36	–	–	–	–	–	–	–
Texture class	*Loam*	*Clay loam*	*Organic*	*Organic*	*Organic*	*Organic*	*Organic*	*Organic*	*Organic*

Summary of mineralogy: Values are reported as percentage (mean ± se), scaled to the total crystalline content and do not reflect the amorphous content. Thus, quartz comprised 79% of the crystalline content and not the total sample. Chesapeake soils were mostly O horizon and therefore had higher amounts of amorphous/OM.

	CRC			PTR			OWC		
	Upland	Transition	Marsh	Upland	Transition	Marsh	Upland	Transition	Marsh
Albite	9.07 ± 0.55	8.03 ± 0.88	6.77 ± 0.09	7.93 ± 0.19	8.2 ± 0.95	7.6 ± 0.4	9.63 ± 0.7	10.43 ± 0.33	8.93 ± 0.26
Chlorite	0	0.47 ± 0.23	0.23 ± 0.23	0	0	0.83 ± 0.2	0.4 ± 0.4	0.1 ± 0.1	0.53 ± 0.27
Gypsum	0	0	0	0	0	0	0	0	0
Halite	0	0	0	0	0	0	0	0	0
Hornblende	0	0	0	0	0	0	0	0	0
Kaolinite	0	5.6 ± 0.1	6.7 ± 0.2	0	2.07 ± 2.07	7.23 ± 0.97	0	0	3.5 ± 1.75
Microcline	6.5 ± 0.8	7.83 ± 0.8	8.57 ± 0.29	6.37 ± 0.68	5.17 ± 0.27	9.03 ± 1.19	6.6 ± 1.19	5.68 ± 0.42	5.9 ± 1.15
Muscovite	20.33 ± 1.67	31.33 ± 1.76	39.67 ± 0.33	21.67 ± 0.88	29.33 ± 1.33	38 ± 1.53	18.33 ± 0.88	20.11 ± 0.75	24.33 ± 0.88
Pyrite	0	0	0	0	0	0	0	0	0
Quartz	63.67 ± 2.19	46.67 ± 1.76	38.33 ± 0.33	63.67 ± 0.88	55.67 ± 2.73	37.67 ± 2.67	65 ± 1.73	63.56 ± 0.53	57 ± 2.52

	GCW			MSM			GWI		
	Upland	Transition	Marsh	Upland	Transition	Marsh	Upland	Transition	Marsh
Albite	1 ± 1	3.03 ± 1.86	1.13 ± 1.13	9.1 ± 1.07	3.37 ± 1.69	0	11.3 ± 2.22	5.83 ± 0.87	2.83 ± 1.5
Chlorite	0	0	0	0	0	0	0	0	0

Table
Continued

	GCW			MSM			GWI		
	Upland	Transition	Marsh	Upland	Transition	Marsh	Upland	Transition	Marsh
Gypsum	0	0	0	0	0	23	0	0	0
Halite	0	0	14.57 ± 4.47	0	0	14	0	0	10.7 ± 3.17
Hornblende	0	0	0	0	0	0	0	0	0
Kaolinite	0	0	11.27 ± 0.93	0	0	14	0	8.4 ± 0.31	0
Microcline	4.67 ± 1.67	5.17 ± 0.95	1.47 ± 1.47	1.37 ± 1.37	1.67 ± 1.67	0	0	2.4 ± 2.4	0
Muscovite	15.33 ± 1.2	18 ± 1.53	34.67 ± 1.2	3.33 ± 3.33	5 ± 5	0	0	19 ± 9.5	10.33 ± 5.36
Pyrite	0	0	2.6 ± 1.38	0	0	0	0	0	0
Quartz	79 ± 2.52	74 ± 2	34 ± 6	86 ± 2.65	90.33 ± 7.31	48	88.67 ± 2.19	64.33 ± 11.46	76.33 ± 7.31

Conflict of Interest

The authors declare no conflicts of interest relevant to this study.

Data Availability Statement

All data and R scripts are available on GitHub (https://github.com/COMPASS-DOE/cmps-soil_characterization) and archived at ESS-DIVE (Patel et al., 2025, https://doi.org/10.15485/2583150). In addition to the O/A surface horizon described in this paper, we also include data for the subsurface B horizon, where available, on ESS-DIVE.

Acknowledgments
This work was supported through the Field, Measurements, and Experiments (FME) component of the Coastal Observations, Mechanisms, and Predictions Across Systems and Scales (COMPASS) project (https://compass.pnnl.gov/). COMPASS-FME is a multi-institutional project supported by the US Department of Energy, Office of Science, Biological and Environmental Research as part of the Environmental System Science Program. This project is led by Pacific Northwest National Laboratory which is operated for DOE by Battelle Memorial Institute under contract DE-AC05-76RL01830. A portion of this research was performed on a project award (60602) from the Environmental Molecular Sciences Laboratory. This work was also supported by the Smithsonian Environmental Research Center. We thank Steven McMurray and Janice Kerns at the OWC/ODNR and Scott Lerberg and Alexander Demeo at CBNERR-VA for facilitating site access. The region of Ohio we are studying is the ancestral homelands of the Seneca, Erie, Kaskaskia and Odawa, as well as places of trade for Indigenous peoples, including the Anishinaabe (Ojibwa, Pottawatomi), Kilatika, Lenape, Kaskaskia, Kickapoo, Miami, Munsee, Peoria, Piankashaw, Shawnee, Wea, and Wyandot. The region of the Chesapeake Bay we are studying is the ancestral homelands of the Cheroenhaka (Nottoway), Chickahominy, Eastern Chickahominy, Mattaponi, Monacan, Nansemond, Nottoway, Pamunkey, Patawomeck, Upper Mattaponi, and Rappahannock tribes.

References

Baker, D. B., Ewing, D. E., Johnson, L. T., Kramer, J. W., Merryfield, B. J., Confesor, R. B., Jr., et al. (2014). Lagrangian analysis of the transport and processing of agricultural runoff in the lower Maumee River and Maumee Bay. *Journal of Great Lakes Research*, *40*(3), 479–495. https://doi.org/10.1016/j.jglr.2014.06.001

Bernhardt, E. S., Blaszczak, J. R., Ficken, C. D., Fork, M. L., Kaiser, K. E., & Seybold, E. C. (2017). Control points in ecosystems: Moving beyond the hot spot hot moment concept. *Ecosystems*, *20*(4), 665–682. https://doi.org/10.1007/s10021-016-0103-y

Bridgham, S. D., Johnston, C. A., Schubauer-Berigan, J. P., & Weishampel, P. (2001). Phosphorus sorption dynamics in soils and coupling with surface and pore water in riverine wetlands. *Soil Science Society of America Journal*, *65*(2), 577–588. https://doi.org/10.2136/sssaj2001.652577x

Byrd, K. B., Windham-Myers, L., Leeuw, T., Downing, B., Morris, J. T., & Ferner, M. C. (2016). Forecasting tidal marsh elevation and habitat change through fusion of Earth observations and a process model. *Ecosphere*, *7*(11), e01582. https://doi.org/10.1002/ecs2.1582

Carter, G. S., Kowalski, K. P., & Eggleston, M. R. (2022). Turbidity and estimated phosphorus retention in a reconnected Lake Erie coastal wetland. *Water*, *14*(12), 1853. https://doi.org/10.3390/w14121853

Chen, H., Rücker, A. M., Liu, Y., Miller, D., Dai, J.-N., Wang, J.-J., et al. (2023). Unique biogeochemical characteristics in coastal ghost forests—The transition from freshwater forested wetland to salt marsh under the influences of sea level rise. *Soil & Environmental Health*, *1*, 100005. https://doi.org/10.1016/j.seh.2023.100005

Chen, Y., & Kirwan, M. L. (2024). Upland forest retreat lags behind sea-level rise in the mid-Atlantic coast. *Global Change Biology*, *30*(1), e17081. https://doi.org/10.1111/gcb.17081

Choquette, A. F., Hirsch, R. M., Murphy, J. C., Johnson, L. T., & Confesor, R. B., Jr. (2019). Tracking changes in nutrient delivery to western Lake Erie: Approaches to compensate for variability and trends in streamflow. *Journal of Great Lakes Research*, *45*(1), 21–39. https://doi.org/10.1016/j.jglr.2018.11.012

Compton, J. E., & Church, M. R. (2011). Salt additions alter short-term nitrogen and carbon mobilization in a coastal Oregon Andisol. *Journal of Environmental Quality*, *40*(5), 1601–1606. https://doi.org/10.2134/jeq2011.0013

Córdova-Kreylos, A. L., Cao, Y., Green, P. G., Hwang, H.-M., Kuivila, K. M., Lamontagne, M. G., et al. (2006). Diversity, composition, and geographical distribution of microbial communities in California salt marsh sediments. *Applied and Environmental Microbiology*, *72*(5), 3357–3366. https://doi.org/10.1128/AEM.72.5.3357-3366.2006

Craft, C. B. (2012). Tidal freshwater forest accretion does not keep pace with sea level rise. *Global Change Biology*, *18*(12), 3615–3623. https://doi.org/10.1111/gcb.12009

Crain, C. M., Silliman, B. R., Bertness, S. L., & Bertness, M. D. (2004). Physical and biotic drivers of plant distribution across estuarine salinity gradients. *Ecology*, *85*(9), 2539–2549. https://doi.org/10.1890/03-0745

Darke, A. K., & Walbridge, M. R. (2000). Al and Fe Biogeochemistry in a floodplain forest: Implications for P retention. *Biogeochemistry*, *51*, 1–32. https://doi.org/10.1023/a:1006302600347

De Feudis, M., Falsone, G., Vianello, G., Agnelli, A., & Vittori Antisari, L. (2022). Soil organic carbon stock assessment in forest ecosystems through pedogenic horizons and fixed depth layers sampling: What's the best one? *Land Degradation & Development*, *33*(9), 1446–1458. https://doi.org/10.1002/ldr.4253

Deng, Y., & Stumm, W. (1993). Kinetics of redox cycling of iron coupled with fulvic acid. *Aquatic Sciences*, *55*(2), 103–111. https://doi.org/10.1007/bf00877439

Ding, J., McDowell, N., Fang, Y., Ward, N., Kirwan, M. L., Regier, P., et al. (2023). Modeling the mechanisms of conifer mortality under seawater exposure. *New Phytologist*, *239*(5), 1679–1691. https://doi.org/10.1111/nph.19076

Ehosioke, S., Adebayo, M. B., Bailey, V. L., Peixoto, R. B., Emmanuel, E. D., Machado-Silva, F., et al. (2024). Geophysical methods reveal the soil architecture and subsurface stratigraphic heterogeneities across land-lake interfaces along Lake Erie. *Journal of Soils and Sediments*, *24*(6), 2215–2236. https://doi.org/10.1007/s11368-024-03787-w

Ellery, S., Ellery, W., Tsikos, H., & Dunlevey, J. (2024). Depression wetland formation by redox-driven iron and silica cycling. *Wetlands Ecology and Management*, *32*(2), 191–206. https://doi.org/10.1007/s11273-023-09968-7

Friedlingstein, P., O'Sullivan, M., Jones, M. W., Andrew, R. M., Gregor, L., Hauck, J., et al. (2022). Global carbon budget 2022. *Earth System Science Data*, *14*(11), 4811–4900. https://doi.org/10.5194/essd-14-4811-2022

Gibbons, K. J., & Bridgeman, T. B. (2020). Effect of temperature on phosphorus flux from anoxic western Lake Erie sediments. *Water Research*, *182*, 116022. https://doi.org/10.1016/j.watres.2020.116022

Golaz, J.-C., Caldwell, P. M., Van Roekel, L. P., Petersen, M. R., Tang, Q., Wolfe, J. D., et al. (2019). The DOE E3SM coupled model version 1: Overview and Evaluation at standard resolution. *Journal of Advances in Modeling Earth Systems*, *11*(7), 2089–2129. https://doi.org/10.1029/2018ms001603

Guimond, J. A., Grande, E., Michael, H. A., Pratt, D., Herndon, E., Noyce, G. L., et al. (2025). The hidden influence of terrestrial groundwater on salt marsh function and resilience. *Nature Water*, *3*(2), 157–166. https://doi.org/10.1038/s44221-024-00384-6

Hanson, P. J., & Walker, A. P. (2020). Advancing global change biology through experimental manipulations: Where have we been and where might we go? *Global Change Biology*, *26*(1), 287–299. https://doi.org/10.1111/gcb.14894

Herbert, E. R., Boon, P., Burgin, A. J., Neubauer, S. C., Franklin, R. B., Ardón, M., et al. (2015). A global perspective on wetland salinization: Ecological consequences of a growing threat to freshwater wetlands. *Ecosphere*, *6*(10), art206-43. https://doi.org/10.1890/es14-00534.1

Herdendorf, C. E., Klarer, D. M., & Herdendorf, R. C. (2006). *The ecology of Old Woman Creek: An estuarine and watershed profile*. National Oceanic and Atmospheric Administration.

Herndon, E. M., Kinsman-Costello, L., Duroe, K. A., Mills, J., Kane, E. S., Sebestyen, S. D., et al. (2019). Iron (oxyhydr)oxides serve as phosphate traps in tundra and boreal peat soils. *Journal of Geophysical Research: Biogeosciences*, *124*(2), 227–246. https://doi.org/10.1029/2018JG004776

Hoitink, A. J. F., & Jay, D. A. (2016). Tidal river dynamics: Implications for deltas. *Reviews of Geophysics*, *54*(1), 240–272. https://doi.org/10.1002/2015RG000507

Holford, I. C. R., & Patrick, W. H., Jr. (1979). Effects of reduction and pH changes on phosphate sorption and mobility in an acid soil. *Soil Science Society of America Journal*, *43*(2), 292–297. https://doi.org/10.2136/sssaj1979.03615995004300020010x

Hopple, A. M., Pennington, S. C., Megonigal, J. P., Bailey, V., & Bond-Lamberty, B. (2022). Disturbance legacies regulate coastal forest soil stability to changing salinity and inundation: A soil transplant experiment. *Soil Biology & Biochemistry*, *169*, 108675. https://doi.org/10.1016/j.soilbio.2022.108675

Howard, L. M., & Lopez, D. L. (2019). World environmental and water resources Congress (pp. 321–333).

Huang, W., & Hall, S. J. (2017). Optimized high-throughput methods for quantifying iron biogeochemical dynamics in soil. *Geoderma*, *306*, 67–72. https://doi.org/10.1016/j.geoderma.2017.07.013

Jordan, T. E., Correll, D. L., & Weller, D. E. (1997). Relating nutrient discharges from watersheds to land use and streamflow variability. *Water Resources Research*, *33*(11), 2579–2590. https://doi.org/10.1029/97WR02005

Kane, D. D., Manning, N. F., & Johnson, L. T. (2022). When it snows it pours: Increased chloride concentrations in the Cuyahoga River during the last half century. *Journal of Great Lakes Research*, *48*(6), 1573–1586. https://doi.org/10.1016/j.jglr.2022.08.017

Kirwan, M. L., & Gedan, K. B. (2019). Sea-level driven land conversion and the formation of ghost forests. *Nature Climate Change*, *9*(6), 450–457. https://doi.org/10.1038/s41558-019-0488-7

Knorr, S., Weisener, C. G., & Phillips, L. A. (2023). The role of agricultural drainage, storm-events, and natural filtration on the biogeochemical cycling capacity of aquatic and sediment environments in Lake Erie's drainage basin. *Science of the Total Environment*, *905*, 167102. https://doi.org/10.1016/j.scitotenv.2023.167102

Krauss, K. W., Duberstein, J. A., Doyle, T. W., Conner, W. H., Day, R. H., Inabinette, L. W., & Whitbeck, J. L. (2009). Site condition, structure, and growth of baldcypress along tidal/non-tidal salinity gradients. *Wetlands*, *29*(2), 505–519. https://doi.org/10.1672/08-77.1

Krieger, K. A. (2003). Effectiveness of a coastal wetland in reducing pollution of a Laurentian Great Lake: Hydrology, sediment, and nutrients. *Wetlands*, *23*(4), 778–791. https://doi.org/10.1672/0277-5212(2003)023[0778:eoacwi]2.0.co;2

Langston, A. K., Kaplan, D. A., & Putz, F. E. (2017). A casualty of climate change? Loss of freshwater forest islands on Florida's Gulf Coast. *Global Change Biology*, *23*(12), 5383–5397. https://doi.org/10.1111/gcb.13805

Li, B., Li, Z., Zheng, J., Jiang, P., Holmquist, J., Regier, P. J., et al. (2024). Integrated effects of site hydrology and vegetation on exchange fluxes and nutrient cycling at a coastal terrestrial-aquatic interface. *Water Resources Research*, *60*(6), e2023WR035580. https://doi.org/10.1029/2023wr035580

Lindsay, W. L. (1988). Solubility and redox equilibria of iron compounds in soils. In *Iron in soils and clay minerals* (pp. 37–62). Springer. https://doi.org/10.1007/978-94-009-4007-9_3

Lowrance, R., Altier, L. S., Newbold, J. D., Schnabel, R. R., Groffman, P. M., Denver, J. M., et al. (1997). Water quality functions of riparian forest buffers in Chesapeake Bay watersheds. *Environmental Management*, *21*(5), 687–712. https://doi.org/10.1007/s002679900060

Maccoux, M. J., Dove, A., Backus, S. M., & Dolan, D. M. (2016). Total and soluble reactive phosphorus loadings to Lake Erie. *Journal of Great Lakes Research*, *42*(6), 1151–1165. https://doi.org/10.1016/j.jglr.2016.08.005

Machado-Silva, F., Weintraub, M. N., Ward, N. D., Doro, K. O., Regier, P. J., Ehosioke, S., et al. (2024). Short-term groundwater level fluctuations drive subsurface redox variability. *Environmental Science & Technology*, *58*(33), 14687–14697. https://doi.org/10.1021/acs.est.4c01115

Maryland-DNR. (2015). Sustainable Forest management plan for Chesapeake Forest lands (No. Revision 9).

McDowell, N. G., Ball, M., Bond-Lamberty, B., Kirwan, M. L., Krauss, K. W., Megonigal, J. P., et al. (2022). Processes and mechanisms of coastal woody-plant mortality. *Global Change Biology*, *28*(20), 5881–5900. https://doi.org/10.1111/gcb.16297

Mehlich, A. (1984). Mehlich 3 soil test extractant: A modification of Mehlich 2 extractant. *Communications in Soil Science and Plant Analysis*, *15*(12), 1409–1416. https://doi.org/10.1080/00103628409367568

Messina, M. G., & Conner, W. H. (1997). *Southern forested wetlands: Ecology and management*. CRC Press.

Michalovicz, L., Dick, W. A., Tormena, C. A., Müller, M. M. L., & Cervi, E. C. (2002). Temporal trends of sulfur levels in soils of northwest Ohio (USA) between 2002 and 2014. *Land Degradation and Development*, *32*(2), 573–582. https://doi.org/10.1002/ldr.3745

Molino, G. D., Carr, J. A., Ganju, N. K., & Kirwan, M. L. (2023). Biophysical drivers of coastal treeline elevation. *Journal of Geophysical Research: Biogeosciences*, *128*(12), e2023JG007525. https://doi.org/10.1029/2023jg007525

Montalvo, M. S., Grande, E., Braswell, A. E., Visser, A., Arora, B., Seybold, E. C., et al. (2024). A fresh take: Seasonal changes in terrestrial freshwater inputs impact salt marsh hydrology and vegetation dynamics. *Estuaries and Coasts*, *47*(8), 1–17. https://doi.org/10.1007/s12237-024-01392-1

Moorhead, D., Bridgeman, T., & Morris, J. (2008). Changes in water quality of Maumee bay 1928–2003. In *Checking the pulse of Lake Erie* (pp. 123–158). Michigan State University Press. https://doi.org/10.14321/j.ctt1bmzpdx.10

Morcos, S. A. (1970). Chemical composition of seawater and the variation of calcium and alkalinity. *ICES Journal of Marine Science*, *33*(2), 126–133. https://doi.org/10.1093/icesjms/33.2.126

Morris, J. T., Drexler, J. Z., Vaughn, L. J. S., & Robinson, A. H. (2022). An assessment of future tidal marsh resilience in the San Francisco Estuary through modeling and quantifiable metrics of sustainability. *Frontiers of Environmental Science and Engineering in China*, *10*, 1039143. https://doi.org/10.3389/fenvs.2022.1039143

Morrissey, E. M., Gillespie, J. L., Morina, J. C., & Franklin, R. B. (2014). Salinity affects microbial activity and soil organic matter content in tidal wetlands. *Global Change Biology*, *20*(4), 1351–1362. https://doi.org/10.1111/gcb.12431

Myers-Pigg, A. N., Pennington, S. C., Homolka, K. K., Lewis, A. M., Otenburg, O., Patel, K. F., et al. (2023). Biogeochemistry of upland to wetland soils, sediments, and surface waters across Mid-Atlantic and Great Lakes coastal interfaces. *Scientific Data*, *10*(1), 822. https://doi.org/10.1038/s41597-023-02548-7

NADP. (2022). NRSP-3. NADP Program office, Wisconsin State laboratory of hygiene (p. 53706).

Noe, G. B., Cashman, M. J., Skalak, K., Gellis, A., Hopkins, K. G., Moyer, D., et al. (2020). Sediment dynamics and implications for management: State of the science from long-term research in the Chesapeake Bay watershed, USA. *WIREs Water*, *7*(4), e1454. https://doi.org/10.1002/wat2.1454

Noe, G. B., Krauss, K. W., Lockaby, B. G., Conner, W. H., & Hupp, C. R. (2013). The effect of increasing salinity and forest mortality on soil nitrogen and phosphorus mineralization in tidal freshwater forested wetlands. *Biogeochemistry*, *114*(1–3), 225–244. https://doi.org/10.1007/s10533-012-9805-1

Ohio, E. P. A. (2012). An overview of ground water quality in Ohio.

Ohio, E. P. A. (2016). *Nutrient mass balance study for Ohio's major rivers*. Ohio Environmental Protection Agency Division of Surface Water.

Oliver, E. E., Houlton, B. Z., & Lipson, D. A. (2021). Controls on soil microbial carbon use efficiency over long-term ecosystem development. *Biogeochemistry*, *152*(2–3), 309–325. https://doi.org/10.1007/s10533-021-00758-y

O'Meara, T. A., Yuan, F., Sulman, B. N., Noyce, G. L., Rich, R., Thornton, P. E., & Megonigal, J. P. (2024). Developing a redox network for coastal saltmarsh systems in the PFLOTRAN reaction model. *Journal of Geophysical Research: Biogeosciences*, *129*(3), e2023JG007633. https://doi.org/10.1029/2023jg007633

Palinkas, C. M., Halka, J. P., Li, M., Sanford, L. P., & Cheng, P. (2014). Sediment deposition from tropical storms in the upper Chesapeake Bay: Field observations and model simulations. *Continental Shelf Research*, *86*, 6–16. https://doi.org/10.1016/j.csr.2013.09.012

Patel, K. F., Fansler, S. J., Campbell, T. P., Bond-Lamberty, B., Smith, A. P., RoyChowdhury, T., et al. (2021). Soil texture and environmental conditions influence the biogeochemical responses of soils to drought and flooding. *Communications Earth and Environment*, *2*, 1–9. https://doi.org/10.1038/s43247-021-00198-4

Patel, K. F., Malhotra, A., Norris, C., McKever, S., Fields, D., Musci, J., et al. (2025). COMPASS-FME synoptic site characterization [Dataset]. *ESS-DIVE*. https://doi.org/10.15485/2583150

Patel, K. F., Rod, K. A., Zheng, J., Regier, P., Machado-Silva, F., Bond-Lamberty, B., et al. (2024). Time to anoxia: Observations and predictions of oxygen drawdown following coastal flood events. *Geoderma*, *444*, 116854. https://doi.org/10.1016/j.geoderma.2024.116854

Petrakis, S., Seyfferth, A., Kan, J., Inamdar, S., & Vargas, R. (2017). Influence of experimental extreme water pulses on greenhouse gas emissions from soils. *Biogeochemistry*, *133*(2), 147–164. https://doi.org/10.1007/s10533-017-0320-2

Ramírez-Flandes, S., González, B., & Ulloa, O. (2019). Redox traits characterize the organization of global microbial communities. *Proceedings of the National Academy of Sciences of the United States of America*, *116*(9), 3630–3635. https://doi.org/10.1073/pnas.1817554116

Regier, P. J., Bond-Lamberty, B., Ward, N., Bailey, V., Bittencourt, R. P., Machado-Silva, F., et al. (2025). Short-term experimental flooding impacts soil biogeochemistry but not aboveground vegetation in a coastal forest. *Proceedings of the National Academy of Sciences of the United States of America*. https://doi.org/10.1073/pnas.2511756122

Regier, P. J., Ward, N. D., Indivero, J., Wiese Moore, C., Norwood, M., & Myers-Pigg, A. (2021). Biogeochemical control points of connectivity between a tidal creek and its floodplain. *Limnology and Oceanography Letters*, *6*(3), 134–142. https://doi.org/10.1002/lol2.10183

Regier, P. J., Ward, N. D., Myers-Pigg, A. N., Grate, J., Freeman, M. J., & Ghosh, R. N. (2023). Seasonal drivers of dissolved oxygen across a tidal creek–marsh interface revealed by machine learning. *Limnology & Oceanography*, *68*, 2359–2374. https://doi.org/10.1002/lno.12426

Regnier, P., Resplandy, L., Najjar, R. G., & Ciais, P. (2022). The land-to-ocean loops of the global carbon cycle. *Nature*, *603*(7901), 401–410. https://doi.org/10.1038/s41586-021-04339-9

Rosentreter, J. A., Borges, A. V., Deemer, B. R., Holgerson, M. A., Liu, S., Song, C., et al. (2021). Half of global methane emissions come from highly variable aquatic ecosystem sources. *Nature Geoscience*, *14*(4), 225–230. https://doi.org/10.1038/s41561-021-00715-2

Sah, R. N., & Mikkelsen, D. S. (1989). Phosphorus behavior in flooded-drained soils. I. effects on phosphorus sorption. *Soil Science Society of America Journal*, *53*(6), 1718–1722. https://doi.org/10.2136/sssaj1989.03615995005300060018x

Saunois, M., Martinez, A., Poulter, B., Zhang, Z., Raymond, P., Regnier, P., et al. (2024). Global Methane Budget 2000–2020. https://doi.org/10.5194/essd-2024-115

Saunois, M., Stavert, A. R., Poulter, B., Bousquet, P., Canadell, J. G., Jackson, R. B., et al. (2020). The global methane budget 2000–2017. *Earth System Science Data*, *12*(3), 1561–1623. https://doi.org/10.5194/essd-12-1561-2020

Sengupta, A., Stegen, J. C., Bond-Lamberty, B., Rivas-Ubach, A., Zheng, J., Handakumbura, P. P., et al. (2021). Antecedent conditions determine the biogeochemical response of coastal soils to seawater exposure. *Soil Biology & Biochemistry*, *153*, 108104. https://doi.org/10.1016/j.soilbio.2020.108104

Seyfried, G. S., Chow, A. T., & O'Halloran, T. L. (2023). Salinization, inundation and tree mortality interact to affect greenhouse gas emissions from stressed coastal forests. *Soil Biology & Biochemistry*, *184*, 109101. https://doi.org/10.1016/j.soilbio.2023.109101

Shiklomanov, A. N., Bond-Lamberty, B., Atkins, J. W., & Gough, C. M. (2020). Structure and parameter uncertainty in centennial projections of forest community structure and carbon cycling. *Global Change Biology*, *26*(11), 6080–6096. https://doi.org/10.1111/gcb.15164

Sinha, E., Bond-Lamberty, B., Calvin, K. V., Drewniak, B. A., Bisht, G., Bernacchi, C., et al. (2023). The impact of crop rotation and spatially varying crop parameters in the E3SM Land Model (ELMv2). *Journal of Geophysical Research: Biogeosciences*, *128*(3), e2022JG007187. https://doi.org/10.1029/2022jg007187

Smith, A. J., & Goetz, E. M. (2021). Climate change drives increased directional movement of landscape ecotones. *Landscape Ecology*, *36*(11), 3105–3116. https://doi.org/10.1007/s10980-021-01314-7

Smith, I. M., Fiorino, G. E., Grabas, G. P., & Wilcox, D. A. (2021). Wetland vegetation response to record-high Lake Ontario water levels. *Journal of Great Lakes Research*, *47*(1), 160–167. https://doi.org/10.1016/j.jglr.2020.10.013

Sulman, B. N., Wang, J., LaFond-Hudson, S., O'Meara, T. A., Yuan, F., Molins, S., et al. (2024). Integrating tide-driven wetland soil redox and biogeochemical interactions into a land surface model. *Journal of Advances in Modeling Earth Systems*, *16*(4), e2023MS004002. https://doi.org/10.1029/2023ms004002

Tank, S. E., Vonk, J. E., Walvoord, M. A., McClelland, J. W., Laurion, I., & Abbott, B. W. (2020). Landscape matters: Predicting the biogeochemical effects of permafrost thaw on aquatic networks with a state factor approach. *Permafrost and Periglacial Processes*, *31*(3), 358–370. https://doi.org/10.1002/ppp.2057

Theuerkauf, E. J., & Braun, K. N. (2021). Rapid water level rise drives unprecedented coastal habitat loss along the Great Lakes of North America. *Journal of Great Lakes Research*, *47*(4), 945–954. https://doi.org/10.1016/j.jglr.2021.05.004

US-DOE. (2017). Research priorities to incorporate terrestrial-aquatic interfaces in Earth System models.

Vahsen, M. L., Todd-Brown, K. E. O., Hicks, J., Pilyugin, S. S., Morris, J. T., & Holmquist, J. R. (2024). Cohort Marsh Equilibrium Model (CMEM): History, mathematics, and implementation. *Journal of Geophysical Research: Biogeosciences*, *129*(4), e2023JG007823. https://doi.org/10.1029/2023jg007823

van Genuchten, M. T. (1980). A closed-form equation for predicting the hydraulic conductivity of unsaturated soils. *Soil Science Society of America Journal*, *44*(5), 892–898. https://doi.org/10.2136/sssaj1980.03615995004400050002x

Viollier, E., Inglett, P. W., Hunter, K., Roychoudhury, A. N., & Van Cappellen, P. (2000). The ferrozine method revisited: Fe(II)/Fe(III) determination in natural waters. *Applied Geochemistry*, *15*(6), 785–790. https://doi.org/10.1016/s0883-2927(99)00097-9

Walker, L. R., Wardle, D. A., Bardgett, R. D., & Clarkson, B. D. (2010). The use of chronosequences in studies of ecological succession and soil development: Chronosequences, succession and soil development. *Journal of Ecology*, *98*(4), 725–736. https://doi.org/10.1111/j.1365-2745.2010.01664.x

Wang, F., Lu, X., Sanders, C. J., & Tang, J. (2019). Tidal wetland resilience to sea level rise increases their carbon sequestration capacity in United States. *Nature Communications*, *10*(1), 5434. https://doi.org/10.1038/s41467-019-13294-z

Wang, W., Zhang, P., Zhang, H., Grossiord, C., Pennington, S. C., Norwood, M. J., et al. (2022). Severe declines in hydraulic capacity and associated carbon starvation drive mortality in seawater exposed Sitka-spruce (Picea sitchensis) trees. *Environmental Research Communications*, *4*(3), 035005. https://doi.org/10.1088/2515-7620/ac5f7d

Ward, N. D., Megonigal, J. P., Bond-Lamberty, B., Bailey, V. L., Butman, D., Canuel, E. A., et al. (2020). Representing the function and sensitivity of coastal interfaces in Earth system models. *Nature Communications*, *11*(1), 2458. https://doi.org/10.1038/s41467-020-16236-2

Ward, N. D., Megonigal, J. P., Weintraub, M. N., Regier, P., Pennington, S. P., Bittencourt Peixoto, R., et al. (2025). A synoptic system for capturing ecosystem control points across terrestrial-aquatic interfaces. *Journal of Geophysical Research: Biogeosciences*. https://doi.org/10.1029/2025JG009335

Weil, R. R., & Brady, N. C. (2016). *The nature and properties of soils, global edition* (15th ed.). Pearson Education.

Weissman, D. S., & Tully, K. L. (2020). Saltwater intrusion affects nutrient concentrations in soil porewater and surface waters of coastal habitats. *Ecosphere*, *11*(2), e03041. https://doi.org/10.1002/ecs2.3041

Wilson, S. J., & Megonigal, J. P. (2025). Nitrate reduction across soils transitioning from coastal forest to wetland are hotspots for denitrification. *Soil Biology & Biochemistry*, *209*, 109904. https://doi.org/10.1016/j.soilbio.2025.109904

Yan, G., Labonté, J. M., Quigg, A., & Kaiser, K. (2020). Hurricanes accelerate dissolved organic carbon cycling in coastal ecosystems. *Frontiers in Marine Science*, *7*, 248. https://doi.org/10.3389/fmars.2020.00248

Yu, C., Xie, S., Song, Z., Xia, S., & Åström, M. E. (2021). Biogeochemical cycling of iron (hydr-)oxides and its impact on organic carbon turnover in coastal wetlands: A global synthesis and perspective. *Earth-Science Reviews*, *218*, 103658. https://doi.org/10.1016/j.earscirev.2021.103658